PLOS PATHOGENS

RESEARCH ARTICLE

Sequential early-life viral infections modulate the microbiota and adaptive immune responses to systemic and mucosal vaccination

Yuhao Li[1], Jerome M. Molleston[2], Crystal Lovato[1], Jasmine Wright[1], Isabel Erickson[1], Duyen Bui[1], Andrew H. Kim[1], Harshad Ingle[1], Somya Aggarwal[1], Lila S. Nolan[3], Ahmed O. Hassan[1], Lynne Foster[1], Michael S. Diamond[1,4,5], Megan T. Baldridge[1,4,6]*

1 Division of Infectious Diseases, Department of Medicine, Washington University School of Medicine, St. Louis, Missouri, United States of America, **2** Division of Pediatric Gastroenterology, Hepatology, and Nutrition, Department of Pediatrics, Washington University School of Medicine, St. Louis, Missouri, United States of America, **3** Division of Newborn Medicine, Department of Pediatrics, Washington University School of Medicine, St. Louis, Missouri, United States of America, **4** Department of Molecular Microbiology, Washington University School of Medicine, St. Louis, Missouri, United States of America, **5** Department of Pathology & Immunology, Washington University School of Medicine, St. Louis, Missouri, United States of America, **6** Edison Family Center for Genome Sciences & Systems Biology, Washington University School of Medicine, St. Louis, Missouri, United States of America

* mbaldridge@wustl.edu

Citation: Li Y, Molleston JM, Lovato C, Wright J, Erickson I, Bui D, et al. (2024) Sequential early-life viral infections modulate the microbiota and adaptive immune responses to systemic and mucosal vaccination. PLoS Pathog 20(10): e1012557. https://doi.org/10.1371/journal.ppat.1012557

Editor: Alexander E. Gorbalenya, Leiden University Medical Center: Leids Universitair Medisch Centrum, NETHERLANDS, KINGDOM OF THE

Received: August 16, 2024

Accepted: September 1, 2024

Published: October 2, 2024

Data Availability Statement: The data from this study are tabulated in the main paper and supplementary materials. The institutional contact from Washington University who can serve as a point of contact for reagent requests would be the Washington University in St. Louis Office of Technology Management, otm@wustl.edu.

Funding: This work was supported by NIH grants R01 OD024917, R01 AI139314, R01 AI141716,

Abstract

Increasing evidence points to the microbial exposome as a critical factor in maturing and shaping the host immune system, thereby influencing responses to immune challenges such as infections or vaccines. To investigate the effect of early-life viral exposures on immune development and vaccine responses, we inoculated mice with six distinct viral pathogens in sequence beginning in the neonatal period, and then evaluated their immune signatures before and after intramuscular or intranasal vaccination against SARS-CoV-2. Sequential viral infection drove profound changes in all aspects of the immune system, including increasing circulating leukocytes, altering innate and adaptive immune cell lineages in tissues, and markedly influencing serum cytokine and total antibody levels. Beyond changes in the immune responses, these exposures also modulated the composition of the endogenous intestinal microbiota. Although sequentially-infected mice exhibited increased systemic immune activation and T cell responses after intramuscular and intranasal SARS-CoV-2 immunization, we observed decreased vaccine-induced antibody responses in these animals. These results suggest that early-life viral exposures are sufficient to diminish antibody responses to vaccination in mice, and highlight the potential importance of considering prior microbial exposures when investigating vaccine responses.

Author summary

Early-life viral infections can shape the host immune system and affect how it responds to vaccines. In this study, we introduced a series of viruses to young mice and then analyzed

R01 AI173360, R21 AI176290, and R21 AI171831 (M.T.B.), R01 AI157155 (M.S.D.), T32 AI007163 (A.H.K. and J.W.), T32 AI106688 and T32 DK077653 (J.M.M.), the Ann W. & Spencer T. Olin-Chancellor's Fellowship (C.L.), and the Dean's Scholars Award from the Washington University Division of Physician-Scientists, which is funded by a Burroughs Wellcome Fund Physician-Scientist Institutional Award (L.S.N.). The funders had no role in study design, data collection and analysis, decision to publish, or preparation of the manuscript.

Competing interests: M.S.D. is a consultant for Inbios, Vir Biotechnology, Ocugen, Topspin Therapeutics, GlaxoSmithKline, Allen & Overy LLP, Moderna, and Immunome. The Diamond laboratory has received unrelated funding support in sponsored research agreements from Vir Biotechnology, Emergent BioSolutions, and Moderna.

their immune systems before and after administering a vaccine for SARS-CoV-2, the virus responsible for COVID-19. We found that these early viral exposures caused significant changes in the immune system, influencing both the types and behaviors of immune cells and the levels of important signaling molecules. Interestingly, while these exposures increased some immune responses, they led to weaker antibody responses to vaccination. This suggests that early viral infections might reduce the effectiveness of vaccines later in life. Additionally, these viral exposures altered the composition of intestinal bacteria, which is known to influence immune health. Our findings highlight the importance of considering early-life infections when studying vaccine responses and immune development.

Introduction

House mice (*Mus musculus*) are regarded as a reliable and versatile model organism for biomedical research, because of their cost-effectiveness and inbred genetics, and availability of a wealth of reagents to characterize them phenotypically. However, over the past decade it has emerged that the limited natural microbial exposure in current specific pathogen-free (SPF) mouse facilities may have important influences on the relevance of research findings [1,2]. Despite having an immune system structured similarly to that of humans, with innate and adaptive components fulfilling similar roles, mice have often poorly replicated transcriptional responses and immune phenotypes seen in humans to the same stimuli, such that pre-clinical results can sometimes fail to predict clinical trial outcomes [3,4]. Unlike humans and wild mice, which are both exposed to a wide variety of microbial influences, laboratory mice raised in SPF environments do not encounter the microbial stimuli found in nature, resulting in differential immune instruction and responses [5–7].

The recent paradigm shift in the understanding that immune phenotypes are potently regulated by complex microbial exposures was brought about in part by various "dirty" mouse models. Cohousing of SPF mice with wild or pet shop-derived mice, rewilding by exposing SPF mice to a natural environment, and "wildling" models in which transferred lab mouse embryos are sired by wild mothers [6,8–12], have provided critical comparisons between "exposed" and naïve SPF mice. These alternative "dirty" models reproduce natural microorganism exposures including bacteria, eukaryotic viruses, bacteriophages, fungi, helminths and/or mites [13,14], and exhibit fundamental shifts in their immune systems, improving their ability to recapitulate essential aspects of human immunity [5,6,8]. Co-housing laboratory mice results in the replication of immune phenotypes and transcriptional signatures found in wild mice or humans, including altering T cell differentiation and modulating susceptibility to new pathogens [6]. Mice rewilded to an outdoors environment also exhibit notable maturation and differentiation within the T cell compartment, accompanied by heightened levels of circulating granulocytes, changes associated with an increase in gut colonization by fungal taxa [9]. Wildling offspring mice also better phenocopy human immune responses to CD28-superagonist and anti-TNF-α treatments than SPF mice [8].

While these microbial transfer models have been useful to identify phenotypes governed by more varied microbial exposures, they are difficult to control due to the varied microbes present in any given pet shop or wild mouse or in the natural environment [2,15]. Furthermore, due to the potential danger of introducing hazardous microbes into animal facilities, experiments utilizing these models generally require specialized, dedicated facilities, which are not available to many investigators. An alternative approach is to instead employ sequential

infection of SPF mice, in which animals are intentionally inoculated with a series of known pathogens. One such model, in which adult SPF mice were infected over time with three viruses and a helminth, demonstrated changes in gene expression that closely approximated pet shop mice as well as adult humans, and exhibited increased inflammatory cytokine responses but blunted antibody responses to yellow fever vaccine [10]. This study suggested that transfer of the gut microbiota is not needed to "humanize" immune responses, but rather, it is the exposure to other pathogens that may be important. However, one challenge of this model was that the infection series was conducted in mice which had already reached adolescence, and was not completed until at least 15 weeks of age. Moreover, helminths themselves have their own microbiota [16,17], which could independently impact immunity. Because the longitudinal microbiota was not profiled in these mice, the response of endogenous microbial communities to a sequential infection regimen remains unclear.

In an effort to develop a tractable sequential infection model for broad laboratory use, as well as to further describe the microbial and immune changes that result from sequential microbial exposures, we devised a virus-only sequential infection model beginning in early life that is completed by 6 weeks of age, allowing mice to be used for further experiments in a rapid and well-controlled manner. We selected viruses encompassing a broad spectrum of viral families, transmission routes, and immune challenges typically encountered in early life [18]. Using this model, we profiled changes in the immune system, identifying marked changes in immune cell populations as well as cytokine and antibody levels. We explored the antibody and T cell response to both intramuscular and intranasal SARS-CoV-2 vaccination in our sequentially-infected mice, and observed a blunted SARS-CoV-2-specific antibody response but enhanced effector T cell response. Finally, we profiled the intestinal microbiome and identified decreases in microbial diversity as well as changes in taxonomic composition associated with sequential viral infection. This tractable model enables the study of a more "microbially-matured" immune system in mice in a rapid and consistent manner in standard animal facilities and implicates early-life virus infections as a regulator of the immune system of SPF mice.

Results

Sequential viral infection creates a durable pro-inflammatory host environment

We sought to develop an "immunologically-mature" murine model in a genetically defined background by utilizing a well-controlled series of microbial exposures, focused exclusively on viruses, that could be rapidly administered to permit further experimental intervention by the age of 10 weeks. Thus, we inoculated C57BL6/J mice with six distinct viruses—murine rotavirus strain EDIM-Cambridge (MRV, 10^4 ID_{50} by oral gavage), murine gamma-herpesvirus 68 (MHV68, 10^5 PFU intranasally), murine norovirus strain CR6 (MNV, 10^6 PFU orally), influenza virus strain PR8 (IAV, 300 PFU intranasally), murine astrovirus (MAstV, infectious fecal filtrate by oral gavage), and coxsackievirus B3 (CVB3, 10^8 PFU orally)—at 1-week intervals beginning when pups were 7 days old (**Fig 1A**). We chose MRV for its relevance to human rotaviruses, which are pervasive enteric viruses which commonly either infect infants through viral exposure or live oral vaccine administration in early life [18]. Herpesvirus infections such as Epstein Barr virus and cytomegalovirus are nearly ubiquitous in humans and often acquired in childhood [19,20], so MHV68 was included to model these latent infections. MNV represents a ubiquitous pathogen in both wild and laboratory mice [21], paralleling the near-universal exposure to noroviruses in children [22,23]. IAV PR8 was selected to model human influenza, a highly-common early-life acute respiratory infection which is also an annual

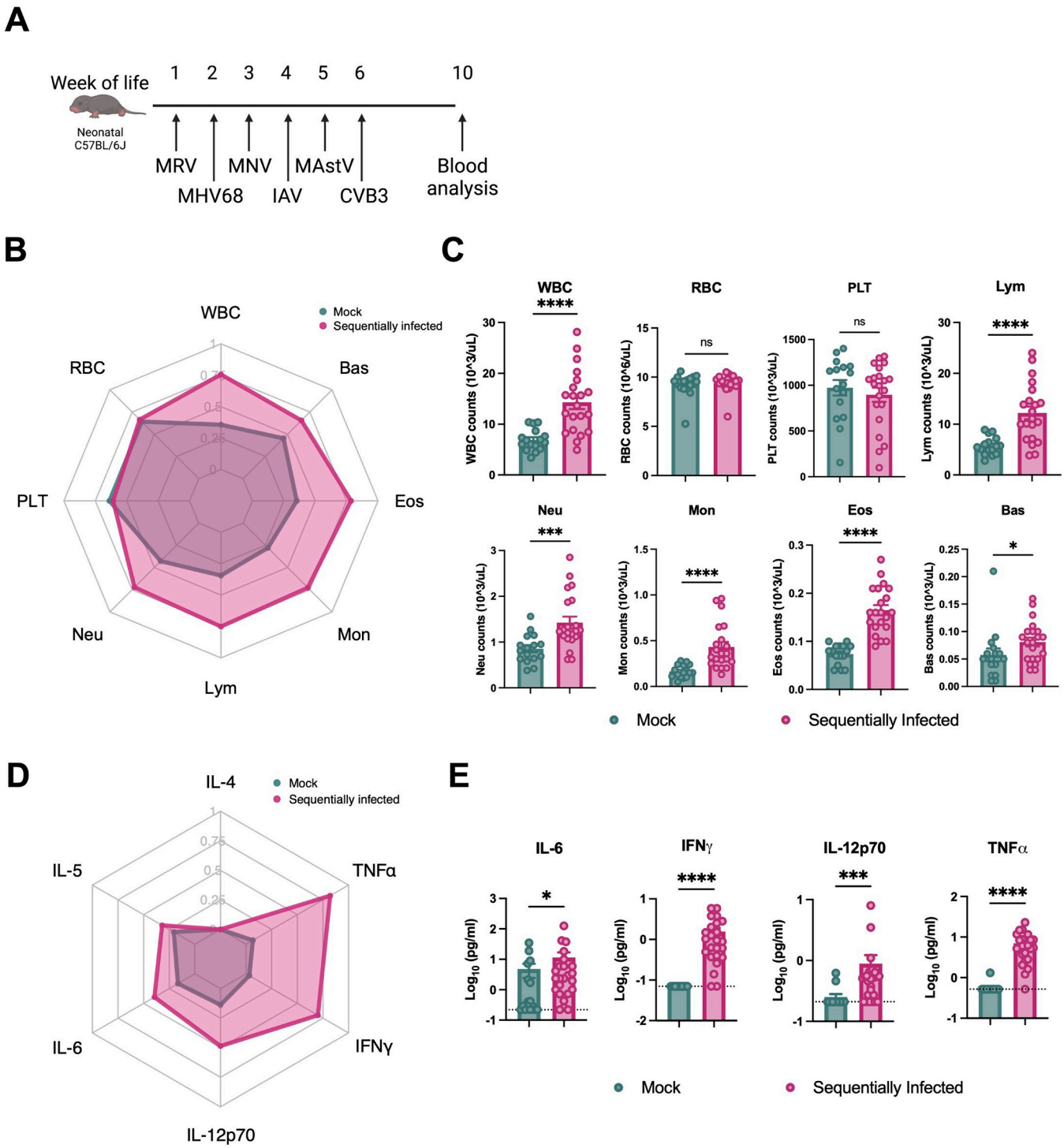

Fig 1. Sequential viral exposure creates an inflammatory host environment. (**A**) Abbreviated sequential infection regimen including murine rotavirus (MRV), murine gammaherpesvirus 68 (MHV68), murine norovirus CR6 (MNV), Influenza A Virus (IAV), murine astrovirus (MAstV), and coxsackievirus B3 (CVB3). Whole blood and indicated tissues of ten-week-old mock- and sequentially-infected C57BL/6J mice were collected for analysis. (**B, C**) Hematologic analysis of peripheral blood using the automatic blood cell counter Element HT5. Radar plot comparing the indicated blood cell populations in mock- (n = 16) and sequentially-infected mice (n = 21) (**B**). White blood cells (WBC), red blood cells (RBC), platelets (PLT), lymphocytes (Lym), neutrophils (Neu), monocytes (Mon), eosinophils (EOS), and basophils (BAS). (**D, E**) Serum was collected from mock- (n = 16) and sequentially-infected (n = 24) mice at the age of 10 weeks. The concentration of cytokines and chemokines was determined by Bioplex assay. Radar plot comparing the serum concentrations of indicated cytokines and chemokines in the indicated groups (**D**). Columns show median values and error bars represent the standard error of the mean, with dotted lines indicating the limit of detection (LOD) of the assays. Undetected cytokines were given a value of LOD. Statistical analysis was performed using unpaired Mann-Whitney test for (**C**) and (**E**): *$p < 0.05$; **$p < 0.01$; ***$p < 0.001$; ****$p < 0.0001$; ns, not significant.

https://doi.org/10.1371/journal.ppat.1012557.g001

vaccine target [24,25]. MAstV is a common enteric virus in mice [26] and was incorporated to reflect human astrovirus infection, which is also nearly ubiquitous in childhood [27,28]. Lastly, CVB3 is an enterovirus that commonly infects humans, used to model highly-prevalent enteroviruses [29,30]. Collectively, these viruses were selected to reflect the multifaceted viral landscape a mammal encounters early in life. All viruses were administered at established inocula [10,31–34] and viral shedding in the stool at expected intervals was confirmed for MRV, MNV, and MAstV (**S1A Fig**). Viral replication of MHV68 was confirmed in the spleen at 7 days post infection, as was viral replication of IAV PR8 in the lungs (**S1A Fig**). Levels of inoculated viruses were also assessed at the 10 week timepoint (**S1B Fig**), at which time MRV and CVB3 were not detectable in fecal samples. However, persistent MNV was still present in the mice, and MAstV was detected in a subset of sequentially-infected mice. Neither IAV nor MHV68 were detected in lung or spleen samples, respectively.

This sequential microbial exposure resulted in global immunological changes in the mice. Hematological analysis at 10 weeks of age revealed a pronounced leukocytosis on a background of preserved red blood cell and platelet counts (**Fig 1B and 1C**). Though the proportions of circulating lymphocytes, neutrophils, monocytes, eosinophils, and basophils were unchanged, their absolute counts were all increased (**Figs 1C and S1C**). These phenotypes were not influenced by sex (**S1D Fig**). Despite similar absolute red blood cell numbers, sequential infection was associated with decreased mean corpuscular hemoglobin (MCH) and mean corpuscular volume (MCV) and increased red cell distribution width (RDW-CV), changes potentially consistent with a chronic pro-inflammatory state (**S1E Fig**)[35].

In addition to circulating immune cells, we also profiled serum cytokine levels, which revealed substantial increases in pro-inflammatory cytokines interleukin (IL)-6 (mean fold change(FC) = 2.39, p = 0.043), IL-12p70 (FC = 3.53, p = 0.002), interferon (IFN)-γ (FC = 22.4, p = 0.001), and tumor necrosis factor (TNF)-α (FC = 12.4, p = 0.001) from sequentially-infected mice at the age of 10 weeks (**Figs 1D, 1E and S1F**). Together, these data demonstrate that sequential viral exposure increased multiple classes of circulating leukocytes and enhanced levels of inflammatory cytokines and chemokines in the serum.

Sequential viral infection modulates the circulating and tissue-resident adaptive immune compartments of laboratory mice

A previous study showed that cohousing of SPF mice with pet shop mice does not alter the frequency and quantity of circulating T cells [5]. In contrast, at 10 weeks of age, mice that had been sequentially-infected with viruses exhibited elevations in the total number of circulating $CD4^+$ and $CD8^+$ T cells (**Figs 2A and S2A**), and this was associated with an enhanced proportion of $CD8^+$ T cells (**S2A Fig**). To assess the impact of sequential viral infection on the differentiation state and distribution of $CD8^+$ T cells, we monitored differentiation markers within the $CD8^+$ T cell subset of peripheral blood mononuclear cells (PBMC) before, during, and after sequential infection. Peripheral blood antigen-experienced ($CD44^{hi}$) $CD8^+$ T cells were rapidly induced in sequentially-infected pups, with many displaying a differentiated effector memory (EM) phenotype ($CD44^{hi}CD62L^{low}$) (**Figs 2B and S3A**). Consistent with the pattern observed in outbred/co-housed mice and humans [5,6,36], sequentially-infected mice exhibited a higher proportion of activated cytotoxic ($GrzB^+$) and terminal effector differentiated ($CD62L^{lo}$, $CXCR3^{lo}$, and $KLRG1^+$) cells within the antigen-experienced ($CD44^{hi}$) $CD8^+$ T cell population (**Fig 2C and S3B**). In contrast, the phenotypes of naïve ($CD44^{lo}$) $CD8^+$ T cells were indistinguishable between mock- and sequentially-infected mice. In addition, cell size (forward scatter, Fsc) and a T cell exhaustion marker (PD1) were equivalent between the two groups (**Fig 2C**).

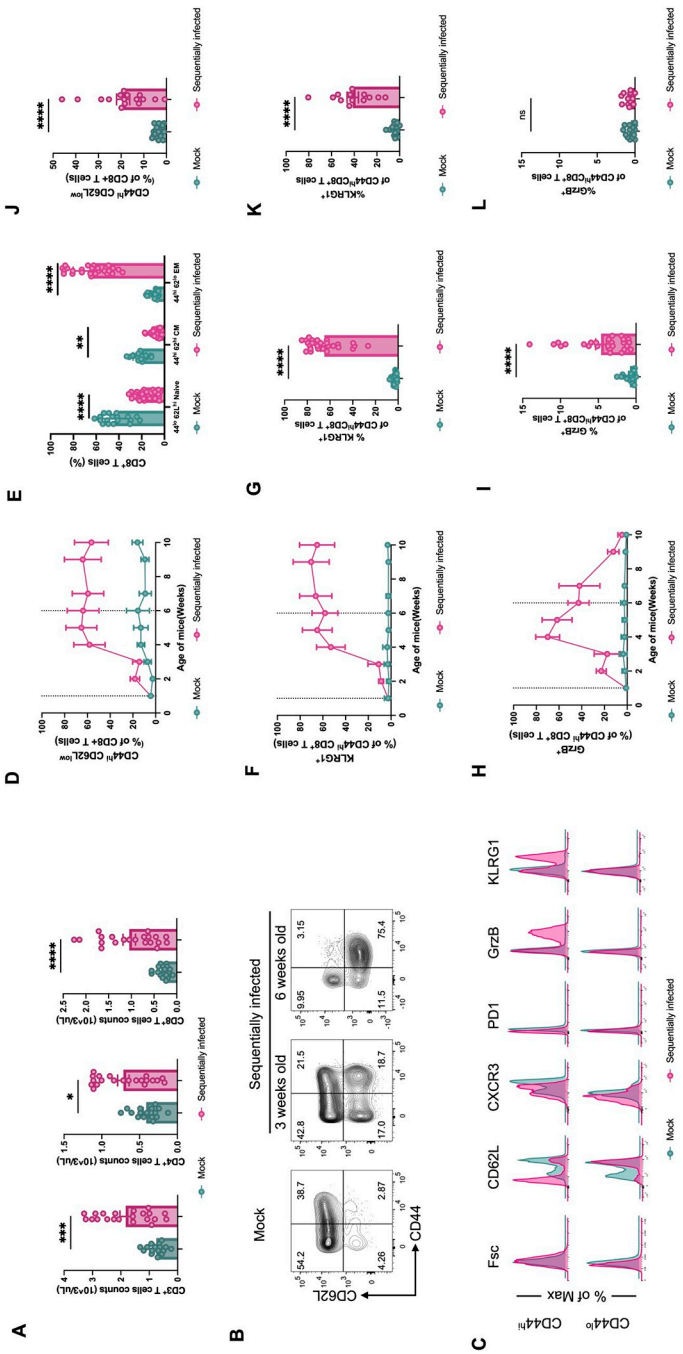

Fig 2. Sequentially infected mice have altered circulating immune cell compositions. (**A**) Peripheral blood T cell counts from mock- (n = 16) or sequentially-infected (n = 21) laboratory mice at the age of 10 weeks. (**B, C**) $CD8^+$ T cell phenotypes in blood from mock- or sequentially-infected laboratory mice. Representative flow plots (n = 18–27) are shown (**B**). Phenotypes of $CD44^{lo}/CD62L^{hi}$ (naive) and $CD44^{hi}$ (antigen-experienced) $CD8^+$ T cells from PBMCs of mock- and sequentially-infected mice compared by flow cytometry (**C**). (**D, E and J**) Frequency of $CD44^{hi}$ (antigen experienced) $CD8^+$ T cells from PBMCs of mock-(n = 18) or sequentially-infected mice (n = 27) from four independent experiments (**D**). Comparison of $CD44^{lo}/CD62L^{hi}$ (Naive), $CD44^{hi}/CD62L^{hi}$ (antigen-experienced central memory, CM), and $CD44^{hi}/CD62L^{lo}$ (antigen-experienced effector memory, EM) $CD8^+$ T cell between mock- and sequentially-infected mice at 10 weeks (**E**) or 7 months (**J**) of age. (**F, G and K**) Frequency of $KLRG1^+$ $CD44^{hi}$ $CD8^+$ T cells from PBMCs of mock- (n = 18) or sequentially-infected mice (n = 27) from four independent experiments (**F**). Comparison of $KLRG1^+$ $CD44^{hi}$ $CD8^+$ T cell between mock- and sequentially infected mice at 10 weeks (**G**) or 7 months (**K**) of age. (**H, I and L**) Frequency of $GrzB^+$ $CD44^{hi}$ $CD8^+$ T cells from PBMCs of mock- mice (n = 18) or sequentially-infected mice (n = 27) from four independent experiments (**H**). Comparison of $GrzB^+$ $CD44^{hi}$

$CD8^+$ T cell between mock- and sequentially-infected mice at 10 weeks (**I**) or 7 months (**L**) of age. Columns show median values and error bars represent the standard error of the mean. Vertical dotted lines indicate the first and last viral inoculations. For (**A**), (**E**), (**F**), (**H**), (**I**), (**K**) and (**L**) statistical analysis was performed using Mann-Whitney test: $^*p < 0.05$; $^{**}p < 0.01$; $^{***}p < 0.001$; $^{****}p < 0.0001$; ns, not significant.

https://doi.org/10.1371/journal.ppat.1012557.g002

Longitudinal analysis revealed that by six weeks of age, the proportion of $CD44^{hi}CD62L^{low}$ EM T cells within $CD8^+$ PBMC increased from 5% to approximately 70%, and subsequently remained relatively stable for the duration of the study (**Figs 2B, 2D and S2B**). At the age of 10 weeks, there were striking differences observed in the populations of naïve, central memory (CM), and terminally differentiated EM $CD8^+$ T cells between the two groups of mice (Fold-change (FC): 6.80, $p < 0.0001$) (**Fig 2E**). These changes in immune cell proportions were consistent across mice of both sexes (**S2C Fig**). Moreover, the population of terminally differentiated EM cells characterized by KLRG1 expression also increased to over 60% in sequentially-infected mice (FC: 21.29, $p < 0.0001$). These $KLRG1^+$ cells persisted in the peripheral blood throughout the study (**Figs 2F, 2G and S2D**). Conversely, the population of $GrzB^+$ effector differentiated memory $CD8^+$ T cells, critical responders against viral infection, returned closer to baseline 4 weeks after the last viral exposure (**Fig 2H**). Nevertheless, sequentially-infected mice still exhibited a higher abundance of $GrzB^+$ cytotoxic T cells compared to mock-infected mice at 10 weeks of age (FC: 5.64, $p < 0.0001$), indicating the persistence of these effector cells despite the observed decrease from peak levels (**Figs 2I and S3E**).

Notably, even at 6 months after viral exposure, sequentially-infected mice exhibited elevated counts of circulating white blood cells ($FC_{10\ weeks} = 2.08$, and $FC_{7\ months} = 1.89$), lymphocytes ($FC_{10\ weeks} = 2.13$, and $FC_{7\ months} = 1.70$), and monocytes ($FC_{10\ weeks} = 2.62$, and $FC_{7\ months} = 1.67$) in sequentially-infected mice, indicating durable effects of these exposures (**S2F Fig**). Sequentially-infected mice also exhibited sustained higher levels of EM $CD8^+$ T cells at 7 months of age ($FC_{10\ weeks} = 6.80$, and $FC_{7\ months} = 5.37$) (**Fig 2J**), with a substantially higher abundance of $KLRG1^+$ cells compared to mock-infected mice, though levels were reduced compared to the 10 week timepoint ($FC_{10\ weeks} = 21.29$, and $FC_{7\ months} = 9.13$) (**Fig 2K**). In contrast, at this later timepoint, no difference was seen between groups in the abundance of GrzB+ cells ($FC_{10\ weeks} = 5.64$, and $FC_{7\ months} = 1.43$) (**Fig 2L**).

We also assessed if our sequential infection protocol would elicit similar immunological effects in adult mice. When viruses are administered starting at 8 weeks of life instead of 1 week, an expansion in the $CD8^+$ T cell EM population is still observed ($FC_{early\ life} = 6.80$, $FC_{adult} = 7.58$) (**S4A Fig**). However, the alterations to the overall peripheral blood white blood cell ($FC_{early\ life} = 2.08$, $FC_{adult} = 1.23$) and lymphocyte ($FC_{early\ life} = 2.13$, $FC_{adult} = 1.21$) populations are less pronounced compared to administration in early life (**S4B Fig**). Thus, early life sequential infection induces robust changes to immune cell populations that are generally durable at least to 6 months of age, and which are more dramatic than when initiated in adulthood.

To gain a more comprehensive understanding of immune status beyond circulating phagocytes and T cells, we analyzed immune cell lineages in mucosal tissues of sequentially-infected mice (**Figs 3A, 3B, S5 and S6**). In contrast to mock-infected mice, which displayed low numbers of $CD8^+$ T cells in nonlymphoid tissues such as the lung and ileum, sequentially-infected mice had notable increases in the abundance of $CD8^+$ T cells in these tissues (**Fig 3A and 3B**). Conversely, the number of mucosal regulatory T cells (Treg) and innate lymphoid cells (ILCs) were generally reduced after sequential infection in the lung but not in the ileum (**Figs 3A, 3B and S6A**). The mesenteric lymph node, the draining lymph node for the intestine, did not exhibit substantial changes in cell populations (**S6B Fig**).

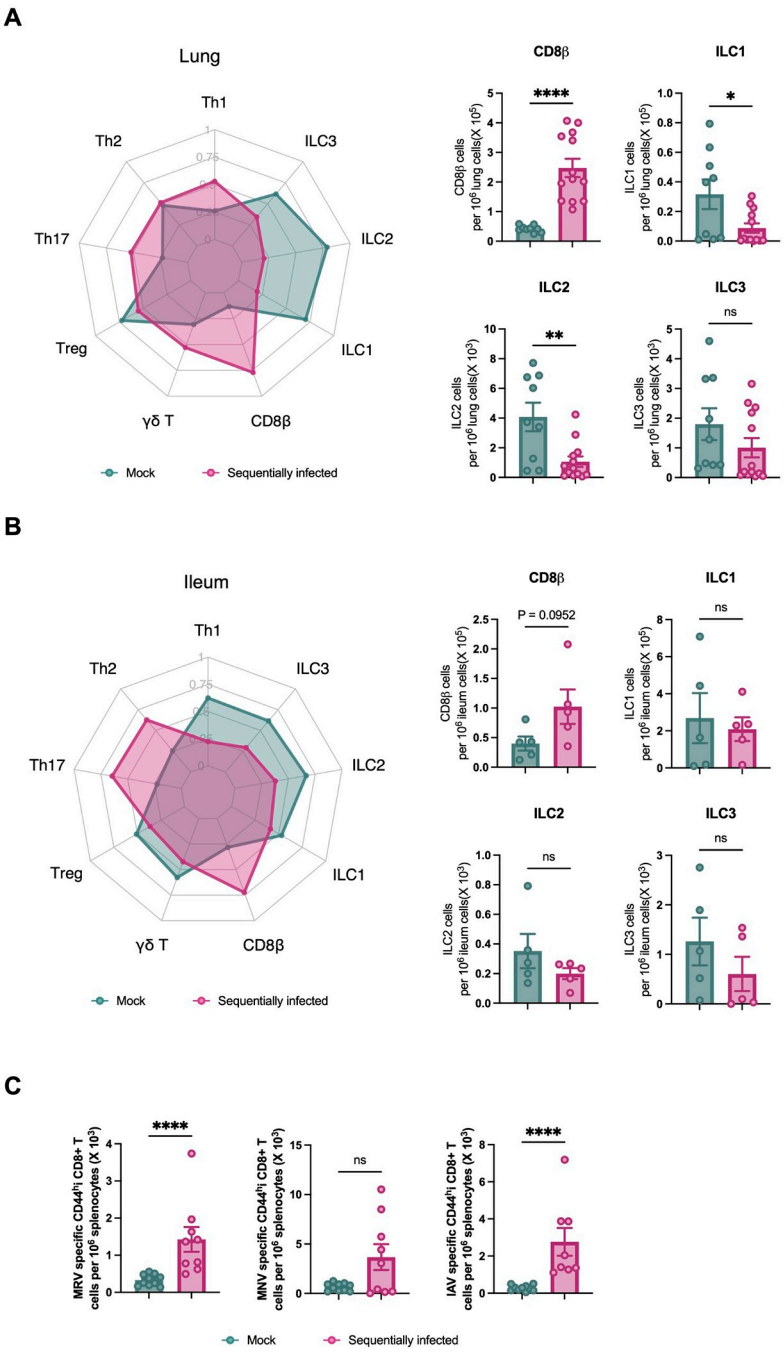

Fig 3. Sequential viral exposure shapes immune cell profiles in mucosal tissues. (**A,B**) Cell types isolated and enumerated by flow cytometry from the lung (**B**) and ileum (**C**) of mock- and sequentially-infected 10 week-old mice (n = 13/group); also shown in S4 Fig. ILC, innate lymphoid cells; T_h, CD4 T helper cells; T_{reg}, regulatory CD4 T cells; γδ T, gamma delta T cells. Radar plot comparing the indicated immune cell populations in mock- and sequentially-infected mice. Single-positive staining for T-bet, Gata3, and Rorγt were used to determine Th1, Th2, and Th17 lineages, respectively. (**C**) Antigen specificity was assessed and enumerated by flow cytometry from the spleens of mock-infected (n = 10) and sequentially infected (n = 9) laboratory mice at 10 weeks of age. Columns show median values and error bars represent the standard error of the mean. Statistical analysis was performed using unpaired Mann-Whitney test: *$p < 0.05$; **$p < 0.01$; ***$p < 0.001$; ****$p < 0.0001$; ns, not significant.

https://doi.org/10.1371/journal.ppat.1012557.g003

To better understand the antigen specificity of these expanded populations of CD8+ T cells, we used well-established MHCII tetramers for MRV[37], MNV [38], and IAV [39] to evaluate virus-specific splenic T cells in mice at 10 weeks of age (**Figs 3C and S5A**). As expected, we identified an increased absolute number of MRV- and IAV-specific CD8+ T splenocytes, indicating that virus-specific T cells contribute at least in part to the overall CD8+ T cell expansion in these infected mice. MNV strain CR6 is known to induce a limited virus-specific CD8+ T cell response, consistent with our findings [38,40].

Beyond these changes in T cell populations, we next evaluated how sequential infection modulated antibody and B cell levels. We measured levels of total antibodies in serum, and found that all IgG subclasses as well as IgM and IgE, but not IgA, were substantially increased in sequentially-infected mice (**Fig 4A**). ELISA results indicated high levels of IgG specific for each of the inoculated viruses in these sequentially-infected mice, supporting virus-specific antibodies as a contributor to increased total IgG levels (**Fig 4B**). However, this increase in total antibodies in sequentially-infected mice was associated with reductions in splenic populations of immature B cells, B1 cells, and plasma cells, whereas germinal center (GC) B cells were increased (**Figs 4C and S6C**). While the proportion of hematopoietic progenitors within the $Lin^{-}Sca1^{+}c\text{-}Kit^{+}$ (LSK) fraction of the bone marrow (BM) was higher in sequentially-infected mice, frequencies of mature and immature B cells as well as B cell progenitors remained comparable (**Figs 4D and S6C**). Taken together, these findings indicate that sequential infection augments both circulating and tissue-resident lymphocytes and antibody levels. Importantly, these phenotypes persisted for 4 weeks following the last exposure, indicating an enduring impact on immune homeostasis.

Sequential viral infection modulates the intestinal microbiome

To evaluate the impact of sequential viral infection on the composition of major microbial niches, 16S ribosomal RNA (rRNA) gene profiling of the intestine and complete nasal turbinate (CNT) was surveilled from mock and sequentially infected mice at 9 weeks of age. A total of 43 fecal samples and 17 CNT samples were subjected to 16S rRNA amplicon sequencing, resulting in 324,493 and 23,088 reads, respectively. By employing dada2 for amplicon sequence variant (ASV) resolution and subsequent taxonomic assignment, we identified 250 distinct ASVs from the fecal samples and 107 distinct ASVs from the CNT samples (**S7A and S7B Fig**). Fecal samples obtained from sequentially-infected mice demonstrated a reduction in bacterial richness (Observed, the number of unique ASVs per sample) and diversity (Shannon, measure of both the number of unique ASVs and their evenness or distribution within sample) when compared to samples from mock-infected mice (**Fig 5A**, Observed: $p = 0.0084$; Shannon: $p = 0.033$). Intestinal bacterial evenness, assessed by Pielou's evenness, was comparable between the two groups ($p = 0.69$). Conversely, no significant differences in alpha diversity parameters were observed in the samples collected from the CNT (**Fig 5A**; $p = 0.39$, 0.59, and 0.81 for Observed, Shannon, and Pielou indices, respectively). Principal coordinates analysis (PCoA) revealed distinct intestinal microbiota compositions between sequentially-infected mice and mock-infected mice (**Fig 5B,** PERMANOVA: $p = 0.036$). In contrast, no distinct clustering was observed in the CNT microbiota (**Fig 5B,** PERMANOVA: $p = 0.68$).

To further explore potential differences in the bacterial communities between mock- and sequentially-infected groups, we performed Kruskal-Wallis rank sum tests and linear discriminant analysis (LDA) based on ASV abundances. These analyses revealed differentially-abundant taxa between the two groups (**Fig 5C**). Specifically, the relative abundances of *Duncaniella* ($p = 0.001$, fdr = 0.023), *Clostridium sensu stricto* ($p = 0.011$, fdr = 0.007), and an unclassified genus belonging to the *Barnesiellaceae* family ($p = 0.0007$, fdr = 0.019) were higher

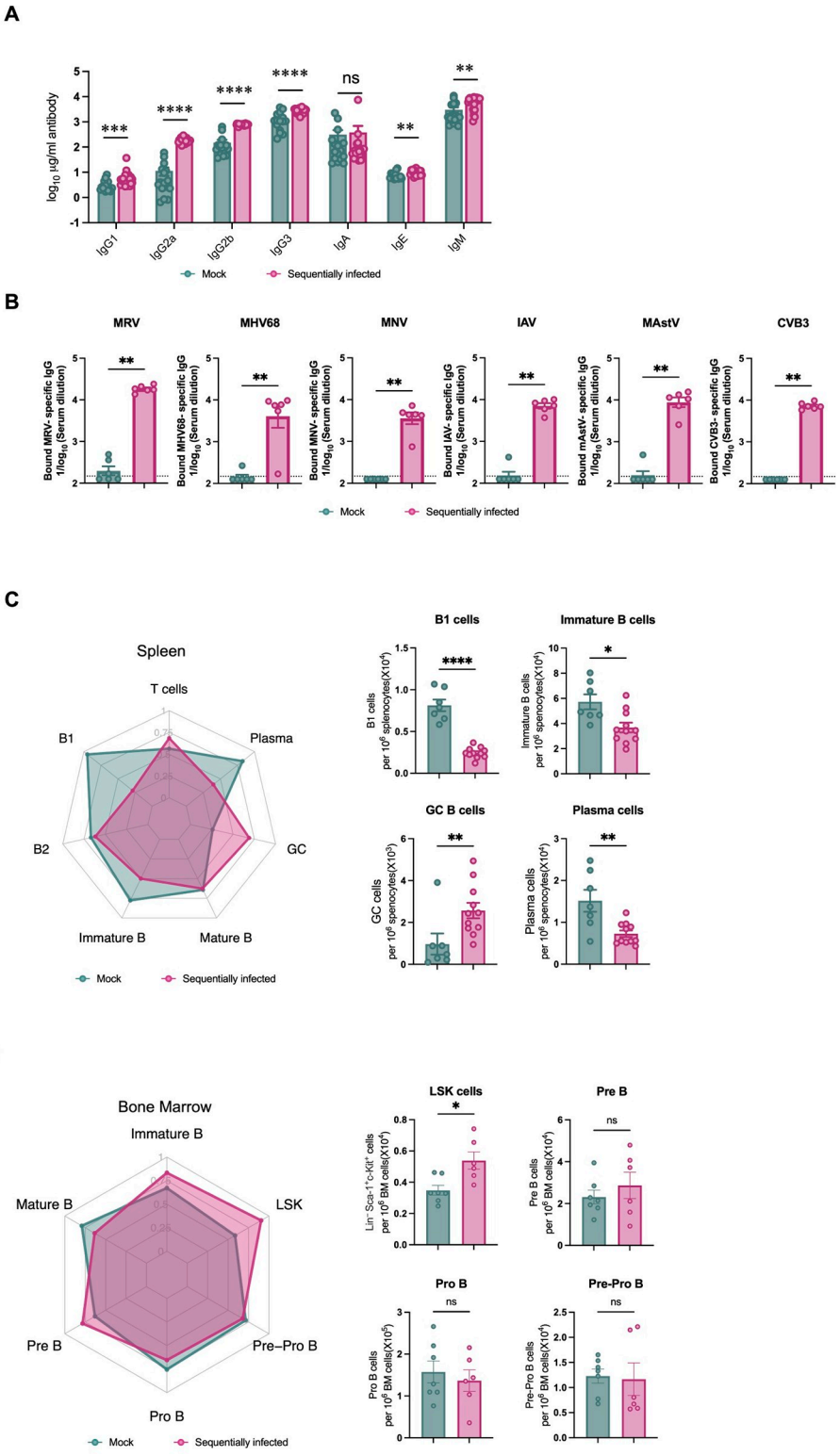

Fig 4. Sequential viral exposure modulates antibody levels and B cell lineages in tissues. (**A**) Total antibody concentrations in serum of mock- (n = 16) and sequentially-infected mice (n = 24) at 10 weeks of age. (**B**) Virus-specific total IgG levels in serum of mock- (n = 16) and sequentially-infected mice (n = 24) at 10 weeks of age. (**C, D**) Cell types isolated and enumerated by flow cytometry from the spleen (**C**) and bone marrow (BM) (**D**) of mock- and sequentially-infected mice. Radar plot comparing the indicated immune cell populations in mock- and sequentially-

infected mice. Columns show median values and error bars represent the standard error of the mean. Statistical analysis was performed using unpaired Mann-Whitney test: *p < 0.05; **p < 0.01; ***p < 0.001; ****p < 0.0001; ns, not significant.

https://doi.org/10.1371/journal.ppat.1012557.g004

in the intestinal microbiota of sequentially-infected mice (**Figs 5C, 5D and S7C**). Conversely, the intestinal microbiota of sequentially-infected mice exhibited reduced relative abundances of *Paramuribaculum* (p = 0.007, fdr = 0.058), *Turicibacter* (p = 0.002, fdr = 0.031), *Alistipes* (p = 0.007, fdr = 0.058), *Oscillibacter* (p = 0.048, fdr = 0.197), *Schaedlerella* (p = 0.035, fdr = 0.153), *Kineothrix* (p = 0.024, fdr = 0.119), *Bifidobacterium* (p = 0.0004, fdr = 0.018), and an unclassified genus belonging to the *Prevotellaceae* family (p = 0.023, fdr = 0.119) (**Figs 5C, 5D and S7C**). In the CNT, only the relative abundance of *Faecalibaculum* (p = 0.012, fdr = 0.47) was decreased in sequentially-infected mice (**Figs 5C and S7D**). These findings indicate that our sequential viral exposure regimen modulates the composition of the intestinal microbiota, with minimal effects on the CNT microbiota, of SPF mice.

Sequential viral infection limits antibody responses and enhances T cell responses to a SARS-CoV-2 vaccine administered by intramuscular or intranasal routes

We next sought to functionally evaluate how early-life microbial exposures influenced responses to a subsequent immune challenge. We used a recently-developed chimpanzee adenovirus-vectored vaccine encoding a prefusion stabilized spike protein (ChAd-SARS-CoV-2-S)[41] that is currently deployed in India (iNCOVACC) and can be readily administered by intramuscular (IM) or intranasal (IN) routes, thereby permitting characterization of effects on systemic and mucosal immunity. At 10 weeks of age, we administered a single 10^{10} viral particle dose of ChAd-SARS-CoV-2-S to mice that had been sequentially-infected or mock controls. Serum samples were collected 4 weeks after immunization, and IgG and IgA responses against purified S proteins were evaluated by enzyme-linked immunosorbent assay (ELISA). While the ChAd-SARS-CoV-2-S vaccine elicited robust levels of S-specific IgG in both mock- and sequentially-infected mice, the S-specific IgG responses in sequentially-infected mice were lower (IM: fold change(FC) = 0.53, p = 0.02; IN: FC = 0.55, p = 0.005) regardless of route of vaccination (**Fig 6A and 6B**). Consistent with a previous report [41], we observed that IM administration of the ChAd-SARS-CoV-2-S vaccine did not induce S-specific serum IgA in either group (**Fig 6A**). In contrast, IN immunization with ChAd-SARS-CoV-2-S elicited S-specific IgA in both groups, but this too was reduced in sequentially-infected mice (**Fig 6B**). We further evaluated the serum neutralization activities against a pseudotype VSV virus displaying the SARS-CoV-2 Wuhan spike [42]. While the sequentially-infected IM immunized animals exhibited similar levels of serum neutralization activity compared to mock controls, the IN immunization group showed reduced serum neutralization antibodies in sequentially infected mice, suggesing a potential decrease in antibody-mediated protection against SARS-CoV-2 (**Fig 6C**).

To evaluate vaccine-induced T cell responses, splenocytes and lung cells were harvested 5 weeks post-vaccination and stimulated *ex vivo* with a pool of 253 overlapping 15-mer S peptides pool as previously described [43]. Following *ex vivo* peptide re-stimulation, we observed a higher number of splenic $CD8^+$ T cells expressing GrzB in sequentially-infected mice that received IM immunization (**Figs 6D and S7**). This finding suggests that microbial exposure enhances the cytotoxic potential of $CD8^+$ T cells, potentially enabling them to better eliminate infected cells. However, there were no significant increases observed in the numbers of $CD8^+$ T cells expressing IFN-γ or $CD4^+$ T cells expressing GrzB, indicating that sequential infection

Fig 5. Sequential viral infection modulates the intestinal bacterial microbiome. The bacterial microbiome of mock- and sequentially-infected mice was profiled for fecal samples (mock-: n = 17, sequentially-infected: n = 26), and complete nasal turbinate tissues (mock-: n = 6, sequentially-infected: n = 11) using sequencing of the 16S rRNA gene. (**A**) Mean values and interquartile ranges of alpha diversity indices. Bacterial richness (Observed), Shannon diversity (Shannon), and Pielou's evenness (Pielou) are shown. Mann-Whitney test: *$p < 0.05$; **$p < 0.01$; ***$p < 0.001$;

****$p < 0.0001$; ns, not significant. (**B**) Principal coordinates analysis (PCoA) using weighted UniFrac distances was performed. Differences between groups were assessed using PERMANOVA. (**C**) Linear discriminant analysis (LDA) effect size analysis was conducted to identify discriminant taxa between the intestinal and complete nasal turbinate microbiomes of mock- and sequentially-infected mice. In the left panel, the LDA effect size (with a 95% confidence interval) is displayed for taxa that were found to be distinct between groups. On the right panel, the false discovery rate (FDR) of each taxa is depicted, with vertical dotted line indicating an FDR of 0.05. (**D**) The relative abundance of discriminant taxa with low FDR identified from the intestinal microbiota at the genus level. Analyzed by Wilcoxon-Mann-Whitney test: **$p < 0.01$; ***$p < 0.001$.

https://doi.org/10.1371/journal.ppat.1012557.g005

may not globally affect the polyfunctionality of these cellular subsets after IM vaccination. In contrast, after IN immunization, we observed an increase in the frequency of splenic IFN-γ-expressing $CD8^+$ T cells, as well as GrzB-expressing $CD4^+$ and $CD8^+$ T cells, in sequentially-infected mice (**Fig 6E**). This suggests that sequential microbial exposure enhances the activation and effector functions of the T cell subsets, particularly following IN vaccination.

In evaluating cells from the lung, we observed a statistically significant increase in the frequency of GrzB-producing $CD8^+$ T cells in sequentially-infected mice that received IM vaccination (**Fig 6F**). However, the frequency of IFN-γ- secreting, antigen-specific $CD103^+CD69^+CD8^+$ T cells within this subset remained relatively low (**Fig 6G**). This indicates that although the overall presence of lung-resident memory T cells was augmented, their capacity to produce IFN-γ in response to antigen stimulation was not altered for IM vaccination. However, upon *ex vivo* re-stimulation of lung cells from sequentially-infected mice following IN immunization, a notable increase in the population of T cells producing both IFN-γ and GrzB was observed (**Fig 6H**). Thus, although the baseline frequency of IFN-γ-secreting, antigen-specific resident memory T cells was initially low, their functionality and capacity to produce cytokines were enhanced by sequential infection. Furthermore, the increase in the frequency of IFN-γ-secreting, antigen-specific $CD103^+CD69^+CD8^+$ T cells in the lung (**Fig 6I**), supports the notion that sequential infection promotes the generation of tissue-resident memory T cells with enhanced cytokine secretion capacity in IN-vaccinated mice. Overall, these findings indicate that repeated viral exposures impact responses to vaccination by blunting vaccine-specific antibody responses and potentially enhancing antigen-specific T cell responses particularly following mucosal exposure. These findings highlight the importance of considering exposure history in evaluating preclinical interventions, as well as the immunological consequences of early-life viral infections.

Discussion

While the efficacy of vaccines relies on antibody- and immune cell-mediated responses, the magnitude of these responses varies across individuals [44–46]. Those residing in high-income countries (HICs) often display a more potent immune response to vaccination than those in low-income and middle-income countries (LMICs) [47]. These distinctions in immunological reactions have been noted for vaccines against influenza, yellow fever, and Ebola [48–50]. Differential microbiota composition and diversity between HICs and LMICs, as well as differential microbial exposure histories, have been implicated as potentially driving these differential vaccine responses [47, 51]. Perturbation of the gut microbiome with antibiotics as well as viral co-infections can have important effects on human vaccine responses [52–55]. The initial state of the intestinal microbiota has also been linked to the immunogenicity of and adverse effects associated with SARS-CoV-2 vaccines [56]. Furthermore, the utilization of probiotics such as *Lactobacillus* and *Bifidobacterium* has exhibited potential in augmenting immune responses to vaccines [57–59]. However, the precise identity of intestinal microbes or prior infections that

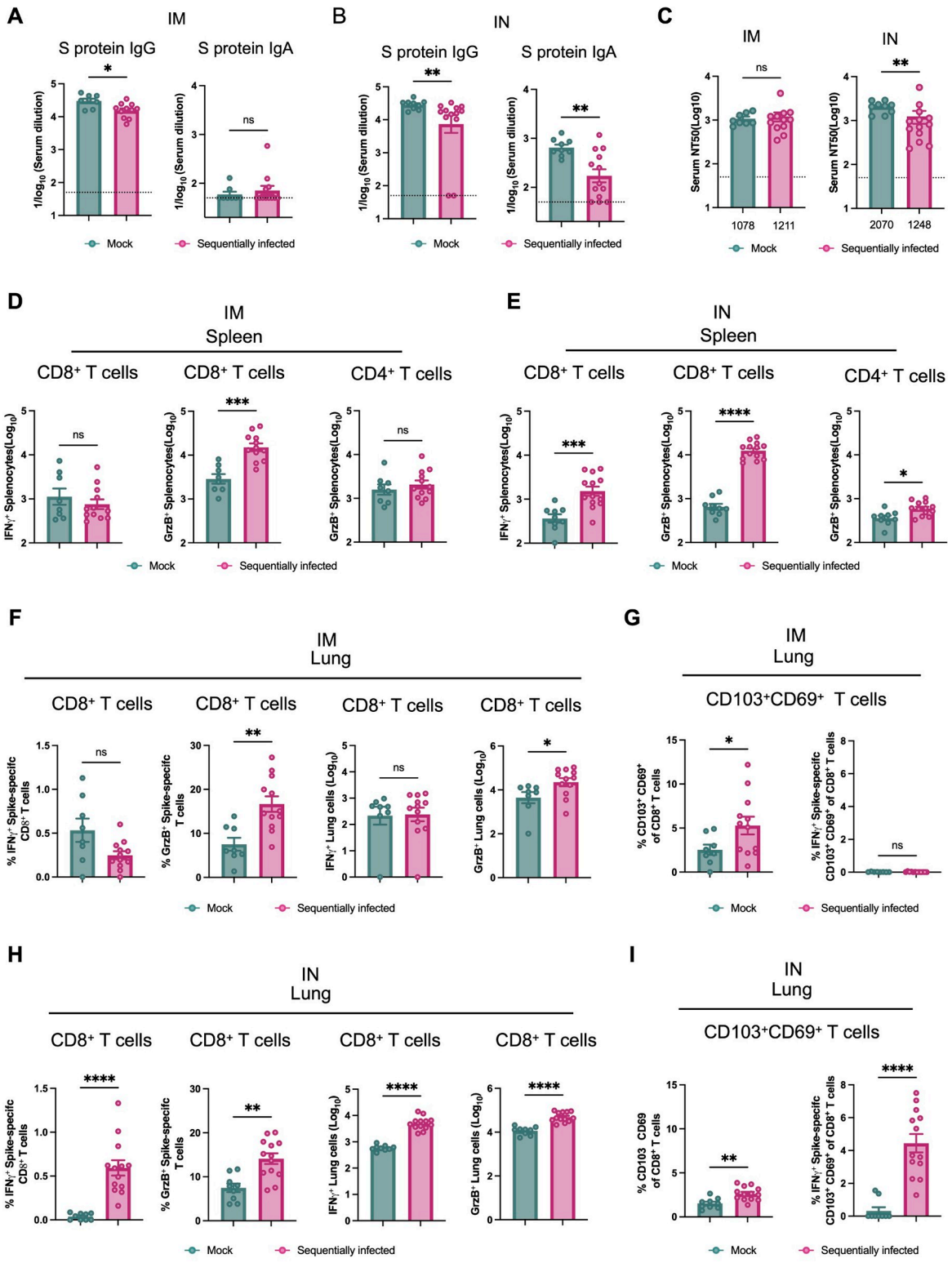

Fig 6. Sequential viral infection is associated with reduced antibody response to intramuscular and intranasal ChAd-SARS-CoV-2 vaccination. (**A, B**) Antibody responses in sera of immunized mice at day 28 after priming were evaluated. Anti-Spike IgG and IgA levels were measured by ELISA in intramuscular (**IM**) or intranasal (**IN**) vaccination studies. Data are pooled from two experiments (n = 8–13). (**C**) Neutralizing activity of serum from immunized mice against pseudoviruses expressing Wuhan-1 spike proteins (numbers below indicate Geometric Mean Titer values; dotted lines show the LOD; values at the LOD are plotted slightly below the LOD). (**D, E**) Cell-

mediated immune responses were analyzed at day 35 post-immunization after re-stimulation with an S protein-peptide pool. Splenocytes were assayed for IFN-γ and GrzB expression in $CD8^+$ T cells and GrzB only in $CD4^+$ T cells by flow cytometry. Cell counts of positive splenocytes in intramuscular (**D**) or intranasal (**E**) vaccination studies (n = 8–13). (**F—I**) Lung $CD8^+$ T cells from intramuscularly (**F, G**) or intranasally (**H, I**) vaccinated mice were assayed for IFN-γ and GrzB expression by flow cytometry after re-stimulation with an S protein peptide pool. Lung $CD8^+$ T cells were phenotyped for expression of CD103 and CD69 after intramuscular (**G**) or intranasal (**I**) vaccination. Columns show median values and error bars represent the standard error of the mean. Dotted lines indicate the LOD of the assays. Mann-Whitney test: $^*p < 0.05$; $^{**}p < 0.01$; $^{***}p < 0.001$; $^{****}p < 0.0001$; ns, not significant.

https://doi.org/10.1371/journal.ppat.1012557.g006

may influence vaccine effectiveness, as well as the mechanisms underlying this influence, remain enigmatic.

Rodent models with heightened microbial exposures, either via cohousing with "dirty" mice or via sequential infection [13], have been shown to exhibit diminished humoral responses to vaccination [10,12]. In this study, we investigated the effects of sequential viral infections in early life on the immune system, vaccine responses, and microbiota of laboratory mice. Six distinct viral exposures resulted in profound and durable changes to the immune system of the mice, including changes in the number and differentiation of white blood cells, increased pro-inflammatory cytokines and total antibodies in serum, and altered peripheral blood antigen-experienced $CD8^+$ T cells. The differentiation of $CD8^+$ T cells was rapidly induced and antigen-experienced $CD8^+$ T cells increased to approximately 70% of peripheral blood mononuclear cells, with no evidence of T cell exhaustion. Single-dose immunization of SARS-CoV-2 stabilized S-protein based vaccine of sequentially-infected mice resulted in enhanced antigen-specific $CD8^+$ T cell responses but decreased antibody responses for both IM and IN routes, including limiting elicitation of neutralizing antibody responses after IN vaccination. In addition, we observed changes to the intestinal microbiota associated with sequential viral infection, despite the absence of any direct modulation of intestinal bacterial populations.

Our findings parallel those observed in immune characterization of other "dirty" mouse models [6]. As in our model, SPF mice cohoused with pet shop mice display decreased antibody responses to vaccination [12]. The elevated cytokines seen in our sequentially infected mice are similar to those seen in "wildling" models as well as to a prior sequential infection model utilizing viruses and a helminth [8,10]. Our study suggests that many major immune phenotypes observed in "dirty" mouse models could be driven by transmission of viral infections including astroviruses and enteroviruses, which has been recently documented as an important consequence of cohousing with pet shop mice [15]. Indeed, our observation of an altered intestinal bacterial microbiota secondary to sequential infection also supports that either viral infection itself or the indirect effects of induced immune responses may contribute to modulation of endogenous microbial communities observed in other "dirty" models.

Our sequential infection model presents a novel approach to immuno-microbiological research by simulating the complex virological landscape encountered by mammals early in life. Distinct from the "dirty" mouse models which incorporate a wide array of uncontrolled microbial exposures, our model employs a series of targeted viral infections, each chosen to represent the varied viral families routinely encountered by humans. By initiating the infection sequence in neonatal mice, we closely mimic the early-life viral exposures critical for immune system development, a period that has been largely understudied in traditional SPF models. The chosen pathogens provide a controlled yet comprehensive viral milieu that induces a spectrum of immune responses, from mucosal to systemic. While antibody and T cell responses specific to the viral pathogens themselves represent a portion of the elicited response, it remains possible that immune responses to other antigens, such as those in the microbiota, may also be enhanced in this model. This controlled diversity allows us to generate an

immunological profile that is both complex and reproducible, offering a refined tool for probing the intricacies of the immune response to early-life viral challenges. Moreover, by completing the infection regimen by 6 weeks of age, our model enables subsequent experimental interventions at an earlier stage compared to other models, thereby accelerating the research timeline and enhancing the translational value of our findings. Compared to the longer time-course of prior sequential infection models [10], this model is expeditious, with the infection series complete by 6 weeks of life. While there is some overlap in immune responses that can be elicited when this regimen is applied starting in adulthood, exposures beginning in early life appear to drive more drastic changes to the immunological milieu. This model thus permits specific dissection of the microbial factors and host pathways that contribute to these immune phenotypes. While the variable exposures achieved via cohousing of SPF mice with wild or pet shop mice may better model the breadth of immune exposures experienced by humans [14], intentional exposures that appropriately mimic the "average" exposures experienced by humans in HICs or LMICs also could inform our understanding of the diversity of human immune responses. In sum, our model stands as a tractable, scalable, and representative system that advances the fidelity of laboratory mice to human immune development, promising greater translational potential for vaccine and immunotherapeutic research.

There remain several important limitations to this study and unanswered questions that we aim to address in the future. While the current model uses six viruses to mimic a wide range of viral exposures, it is still unknown how each virus contributes to immune maturation and modulation of the intestinal microbiota or affects immunological phenotypes, and indeed if a subset of viruses could be sufficient to drive the observed phenotypes. Two of the viruses used in this study, MHV68 and MNV, establish chronic infection in mice, while the others are self-limited; it is possible that the immune exposure of acute infection is the key event, or that ongoing immune stimulation associated with chronic and latent viral infection may maintain the immune activation seen in this study [40,60]. Chronic infections with helminths, mycobacteria, and hepatitis viruses have been previously reported to limit vaccine efficacy, consistent with our current observations [61]. Furthermore, the importance of the bacterial microbial changes in contributing to the immune maturation we observed is not yet clear. Further investigation is needed to determine whether these changes are a major factor in the altered immune system composition and responses of sequentially-infected mice.

Overall, the results of this study indicate that sequential viral infections modulate the microbiota and lead to changes in the immune system that dampen specific adaptive responses to systemic and mucosal vaccination. This study highlights the importance of early-life microbial exposure and its impact on the immune system and gut microbiota. Sequential infection provides a powerful model for a matured immune system that can be readily leveraged for immunology, virology, and vaccine studies.

Materials and Methods

Ethics statement

Animal studies were carried out in accordance with the recommendations in the Guide for the Care and Use of Laboratory Animals of the National Institutes of Health. The protocols were approved by the Institutional Animal Care and Use Committee at the Washington University School of Medicine (22–0140).

Mice and sequential infections

WT C57BL/6J (stock no. 000664) mice were purchased from Jackson Laboratories and maintained at Washington University School of Medicine under specific-pathogen-free conditions

according to University guidelines. Timed matings were performed, with males subsequently removed from breeding cages. Neonatal mice were initially infected at 7 days of age, while adult mice were initially infected at 8 weeks (56 days) of life. Subsequent infections and analyses were performed as indicated, with all mice weaned from dams at 21 days of life. Weaned mice were then co-housed with up to five mice of the same sex per cage with autoclaved standard chow pellets and water provided *ad libitum*.

Neonatal or adult mice were inoculated with six distinct viral pathogens—murine rotavirus strain EDIM-Cambridge (MRV, 10^4 ID_{50}/mouse), murine gamma-herpesvirus 68 (MHV68, 10^5 PFU/mouse), murine norovirus strain CR6 (MNV, 10^6 PFU/mouse), influenza virus strain PR8 (IAV, 300 PFU/mouse), murine astrovirus (MAstV), and coxsackievirus B3 (CVB3, 10^8 PFU/mouse)—at 1-week intervals beginning when pups were at 1 week of life. Blood and fecal samples were collected for virological, immunological, and microbiota analyses. Four weeks after the last viral exposure, 10-week-old animals were immunized with a single dose of 10^{10} viral particles (vp) of ChAd-SARS-CoV-2-S in 50 μl PBS via intramuscular injection in the hind leg or via intranasal inoculation [41, 62]. Animals were euthanized at 5 weeks post-vaccination, and tissues were harvested for virological, immunological, and pathological analyses.

Blood analysis for hematology

To evaluate the complete blood counts (CBC) from the mock- and sequentially- infected mice, blood was collected via the submandibular vein into EDTA-coated tubes and promptly analyzed using the Heska Element HT5 hematology analyzer (Barrie, Ontario, Canada).

ELISA

For virus-specific IgG evaluation, purified MRV, MHV68, MNV, IAV, MAstV, or CVB3 viral particles were coated onto 96-well Maxisorp clear plates at 2 mg/mL in 50 mM Na_2CO_3 pH 9.6 (70 μL) overnight at 4˚C. For vaccine-specific antibody evaluation, purified SARS-CoV-2 S protein was coated onto 96-well Maxisorp clear plates at 2 mg/mL in 50 mM Na_2CO_3 pH 9.6 (70 μL) overnight at 4˚C. Coating buffers were aspirated, and wells were blocked with 200 μL 1% BSA PBST (Blocking buffer) for 1 h(hour) at 37˚C. The blocked plates then were ready for use after three rounds of PBST washing. Heat-inactivated serum samples were diluted in blocking buffer, and 50 μL of respective serum dilutions were used for the assay. Diluted serum samples were incubated in the blocked ELISA plates for 1 h at room temperature. The ELISA plates were again washed thrice in PBST, followed by the addition of 50 μL of anti-mouse IgG-HRP (1:2000 in PBST) or anti-mouse IgA-HRP (1:2000 in PBST). Plates were incubated at room temperature for 1 h, washed thrice in PBST, and then 1:5000 dilution of streptavidin-HRP (Thermo-Fisher) was added to wells. Following a 1 h incubation at room temperature, plates were washed thrice with PBST, and 50 mL of 1-Step Ultra TMB-ELISA was added (ThermoFisher Cat. #34028). Following a 12 to 15-min incubation, reactions were stopped with 50 mL of 2 M sulfuric acid. The absorbance of each well at 450 nm was read (Synergy H1) within 2 min of the addition of sulfuric acid. Optical density (450 nm) measurements were determined using a microplate reader (Bio-Rad). The endpoint serum dilution was calculated with curve fit analysis of optical density (OD) values for serially diluted sera with a cut-off value set to three times the background signal.

Flow cytometry characterization

Peripheral blood leukocytes, splenocytes, or tissue cells were evaluated by flow cytometry. RBCs were removed from heparinized whole blood or single-cell suspensions using RBC lysis buffer (BioLegend). Isolated mouse cells were surface-stained with antibodies against CD3 (BD Biosciences, 145-2C11,1:200), CD45(Biolegend, 30F-11,1:200), CD11b(Biolegend, M1/

70,1:200), CD11c(Biolegend, N418,1:200), GR1(Biolegend, RB6-8C5,1:200), Ly6G(Biolegend, 1A8,1:200), Ly6C(Biolegend, AL21, 1:200), MHC II (Ia-Ie)(Biolegend, M5/114.15.2, 1:200), CD8α(Biolegend, 53–6.7,1:400), CD4(Biolegend, RM4-5, 1:400), CD62L (Biolegend, MEL-14, 1:200), CD44(Biolegend, IM7, 1:200), CD69(Biolegend, H1.2F3, 1:200), CD103(Biolegend, M290, 1:200), PD-1(Biolegend, RMP1-30, 1:200), KLRG1(Biolegend, 2F1, 1:200), CXCR3(Biolegend, CXCR3-173, 1:200), CD127(Biolegend, SB/199, 1:200), TCR γ/δ (Biolegend, GL3, 1:200), F4/80(BD Biosciences, Cl-A3-1, 1:200), GrzB(Invitrogen, GRB04, 1:200), CD43(Biolegend, 1B11,1:200), IgM(Biolegend, RMM-1,1:200), IgD (Biolegend, 11-26c.2a,1:200,), Ter119 (Biolegend, TER-119,1:200), Gr-1(Biolegend, RB6-8C5,1:400), CD19(Biolegend, 6D5,1:200,), B220(Biolegend, RA3-6B2,1:200), Sca-1(Biolegend, D7,1:200,), c-Kit(eBioscience, 2B8,1:100,). Virus-specific T cells were identified using BV421-labeled MHCII tetramer H2-Kb Rotavirus VP6 VGPVFPPGM [37], H2-Kb murine norovirus CR6 ORF2 519–527 SWVPRLFQL [38], or H-2D(b) Influenza A PA 224–233 SSLENFRAYV [39]. Cell viability was determined using LIVE/DEAD Fixable Aqua Dead Cell Stain Kit (Invitrogen). Intracellular staining for transcription factors was performed using the eBioscience Foxp3 / Transcription Factor Staining Buffer Set (Invitrogen) with antibodies against granzyme B (QA16A02), Foxp3 (FJK-16s), T-bet (4B10), Eomes (Dan11mag), Gata3 (L50-823), Rorγt (Q31-378) following manufacturer's guidelines. Single positive staining for T-bet, Gata3, and Rorγt were used to determine Th1, Th2, and Th17 lineages, respectively. The stained samples were acquired using BD X-20 cytometer and analyzed with FlowJo X 10.0 software.

Peptide restimulation and intracellular cytokine staining

Splenocytes from intramuscularly vaccinated mice were incubated in culture with a pool of 253 overlapping 15-mer SARS-CoV-2 S peptides[43] for 12 h at 37˚C before a 4 h treatment with brefeldin A (BioLegend, 420601). Following blocking with an anti-FcγR antibody (BioLegend, clone 93), cells were stained on ice with CD45 (BD BioSciences, 30-F11, 1:400); CD44, CD4, CD8b, and CD19 (BioLegend, 1:200, respectively), and Fixable Aqua Dead Cell Stain (Invitrogen, L34966). Stained cells were fixed and permeabilized with the Foxp3/Transcription Factor Staining Buffer Set (eBiosciences, 00–5523). Subsequently, intracellular staining was performed with anti-IFN-γ (BD Biosciences, XMG1.2, 1:200), anti-TNF-α (BioLegend, MP6-XT22, 1:200), and anti-GrB (Invitrogen, GRB04, 1:200). Lungs from immunized mice were harvested and digested for 1 h at 37˚C in digestion buffer consisting of RPMI media supplemented with Collagenase (Sigma, 2 mg/ml) and DNase I (Sigma, 0.05 mg/ml). Lung cells were incubated at 37C with the pool of 253 overlapping 15- mer SARS-CoV-2 S peptides described above in the presence of brefeldin A for 5 h at 37˚C. Lung cells then were stained as described above except no CD19 staining was included, and CD103-FITC and CD69-BV711 (BioLegend clones, 2E7, and, H1.2F3, respectively) were added. Analysis was performed on a BD X-20 cytometer, using FlowJo X 10.0 software.

Measurement of serum cytokines, chemokines, and antibodies

Serum cytokines, chemokines, and antibodies were quantitated with the multiplex immunoassay Th1/Th2 panel 6plx (IL-4, IL-5, IL-6, IFN-γ, IL-12p70, and TNF-α) or mouse Antibody Isotyping Panel 7plx (IgG1, IgG2a, IgG2b, IgG3, IgA, IgE, and IgM) using a Luminex 200 with Bio-plex Manager Software 5.0.

Pseudovirus neutralization assay

Vero-TMPRSS2 cells [63] were seeded into 96 well plates in DMEM supplemented with 10% FBS without blasticidin. The next day, serum samples were serially diluted with DMEM

supplemented with 2% FBS and mixed with VSV-eGFP-Wuhan spike pseudoviruses and incubated for 1 h at 37˚C. Antibody-virus complexes were added to Vero-TMPRSS2 cell monolayers and incubated for 1 h at 37˚C. Subsequently, cells were overlaid with 1% (w/v) methylcellulose in MEM. Plates were harvested 20 hours post infection by removing overlays and fixed with 4% PFA in PBS for 20 min at room temperature. Plates were washed and sequentially visualized and quantitated on an ImmunoSpot analyzer (Cellular Technology).

16S rRNA gene Illumina sequencing and analysis

Phenol:chloroform-extracted DNA from fecal pellets was used for both 16S rRNA gene qPCR and sequencing. SYBR green qPCR for the 16S rRNA gene was performed with 515F (5'-GTGCCAGCMGCCGCGGTAA-3') and 805R (5'-GACTACCAGGGTATCTAATCC-3') primers to detect the V4 hypervariable region.

Primer selection and PCRs were performed as described previously [64]. Briefly, each sample was amplified in triplicate with Golay-barcoded primers specific for the V4 region (F515/R806), combined, and confirmed by gel electrophoresis. PCR reactions contained 18.8μL RNase/DNase-free water, 2.5μL 10X High Fidelity PCR Buffer (Invitrogen), 0.5μL 10 mM dNTPs, 1μL 50 mM MgSO4, 0.5μL each of the forward and reverse primers (10 μM final concentration), 0.1μL Platinum High Fidelity Taq (Invitrogen) and 1.0μL genomic DNA. Reactions were held at 94˚C for 2 min to denature the DNA, with amplification proceeding for 26 cycles at 94˚C for 15s, 50˚C for 30s, and 68˚C for 30s; a final extension of 2 min at 68˚C was added to ensure complete amplification. Amplicons were pooled and purified with 0.6x Agencourt Ampure XP beads (Beckman-Coulter) according to the manufacturer's instructions. The final pooled samples, along with aliquots of the three sequencing primers, were sent to the Center for Genome Sciences (Washington University School of Medicine) for sequencing by the 2x250bp protocol with the Illumina MiSeq platform.

Read quality control and the resolution of amplicon sequence variants (ASVs) were performed with the dada2 R package [65]. ASVs that were not assigned to the kingdom Bacteria were filtered out. The remaining reads were assigned taxonomy using the Ribosomal Database Project (RDP trainset 16/release 11.5) 16S rRNA gene sequence database [66]. Ecological analyses, such as alpha-diversity (richness, Faith's phylogenetic diversity) and beta-diversity analyses (unweighted and weighted UniFrac distances), were performed using PhyloSeq and additional R packages [67], and differentially abundant taxa between sample groups were identified by performing pairwise comparisons using LEfSe and MicrobiotaProcess packages [68,69]. 16S rRNA gene sequencing data have been uploaded to the European Nucleotide Archive (accession no. PRJEB65723).

Quantification of viral genomes

RNA was purified from spleen, lungs, and fecal pellets of infected mice using TRIzol chloroform extractions. cDNA was then synthesized from 1 ug of RNA and RT-qPCR was performed using TaqMan reagents. Standards were created using 10^9–10^0 dilutions of gBlocks™ (Integrated DNA Technologies). Primers and probes for MNV [70], MAstV [71], and *Rps29* [72] are as previously reported. For MRV, forward primer 5' CTTCTGGACTACGACAGAC TATTT 3', reverse primer 5' GATCTTTGATCGGTTCGTTGTG 3', and probe 5'—/56-FAM/AGCGCTGCA/ZEN/ACTTAGACTACGAT/3IABkFQ—3' were used to detect NSP3. For MHV68, forward primer 5' GTGTAGAGGGTCCAGGTTAATG 3', reverse primer 5' CTGT TTGCTTCTCCACAGA 3', and probe 5'—/56-FAM/TTCTGGGTT/ZEN/CTGCAGCAAAT GTGC/3IABkFQ– 3' were used to detect ORF50. For IAV PR8, forward primer 5' CATCC TGTTGTATATGAGGCCCAT 3', reverse primer 5' GGACTGCAGCGTAGACGCTT 3', and

probe 5'—/56-FAM/CTCAGTTAT/ZEN/TCTGCTGGTGCACTTGCCA/3IABkFQ– 3' were used.

Statistical analysis

Statistical significance was assigned when P values were <0.05 using Prism Version 8 (GraphPad). Tests, number of animals (n), median values, and statistical comparison groups are indicated in the figure legends. Radar charts were plotted using an R library [73].

Supporting information

S1 Fig. Sequential infection does not alter relative proportions of white blood cells. (**A**) Murine rotavirus (MRV) genome copies detected in fecal pellets of naïve (n = 1) and sequentially infected (n = 3) mice at 7 days post-inoculation. Murine norovirus strain CR6 (MNV) and murine astrovirus (MAstV) genome copies detected in fecal pellets of mock- (n = 18) and sequentially-infected (n = 25) mice at indicated timepoints post-inoculation. Murine gammaherpesvirus (MHV68) ORF50 gene copies were detected in the spleen in naïve (n = 2) and sequentially infected (n = 2) mice at 7 days post-inoculation. Influenza virus strain PR8 (IAV) genome copies were detected in lung tissue in naïve (n = 2) and sequentially infected (n = 2) mice at 7 days post-inoculation. Columns show the mean values, error bars depict standard deviation, and the dotted lines depict the LOD for the assays. Undetectable samples were given a value of LOD. (**B**) MRV, MNV, MAstV, and CVB3 genome copies were detected in fecal pellets of naïve (n = 5) and sequentially infected (n = 7) mice at 10 weeks of age. MHV68 ORF50 gene copies were detected in the spleen of naïve (n = 4) and sequentially infected (n = 4) mice at 10 weeks of age. IAV genome copies were detected in lung tissue in naïve (n = 4) and sequentially infected (n = 4) mice at 10 weeks of age. Columns show the mean values, error bars depict standard deviation, and the dotted lines depict the LOD for the assays. Undetectable samples were given a value of LOD. (**C**) Frequency of lymphocytes (Lym), neutrophils (Neu), monocytes (Mon), eosinophils (Eos), and basophils (Bas) in the hematological analysis of mock- (n = 16) and sequentially-infected (n = 21) mice at 10 weeks of age. (**D**) Separation of CBC data by sex for mock- and sequentially-infected mice. (**E**) Hematological analysis of hematocrit (Hct), hemoglobin (Hgb), mean corpuscular hemoglobin (MCH), mean corpuscular hemoglobin concentration (MCHC), mean corpuscular volume (MCV), mean platelet volume (MPV) and increased red cell distribution width (RDW-CV). (**F**) Serum cytokines IL-4 and IL-5 in mock (n = 16) and sequentially-infected (n = 21) mice at 10 weeks of age. Columns show median values, error bars represent the standard error of the mean, and dotted lines indicate the LOD of the assays. Data are representative of 3 technical replicates. The undetectable samples were given a value of LOD. In A, significance was determined using a two-way ANOVA test with the Geisser_Greenhouse correction; In B, D, and E, significance was determined using unpaired Mann-Whitney test; In C, significance was determined using Dunn's multiple comparisons correct test: $^{*}p < 0.05$;$^{**}p < 0.01$; $^{***}p < 0.001$; $^{****}p < 0.0001$; ns, not significant.
(TIF)

S2 Fig. PBMC T cell subsets vary between mock- and sequentially-infected mice. (**A**) Frequency of PBMC $CD3^+$, $CD4^+$, and $CD8^+$ T cells from mock- (n = 16) or sequentially-infected (n = 21) mice at 10 weeks of age. (**B**) Frequency of $CD44^{hi}$ (antigen-experienced) $CD8^+$ T cells from PBMCs of mock- or sequentially-infected mice between 1 week and 9 weeks of age. (**C**) $CD44^{lo}/CD62L^{hi}$ (Naive), $CD44^{hi}/CD62L^{hi}$ (antigen-experienced central memory, CM), and $CD44^{hi}/CD62L^{lo}$ (antigen-experienced effector memory, EM) $CD8^+$ T cells of mock-infected

and sequentially infected mice, separated by sex. (**D**) Frequency of $KLRG^{+}$ $CD44^{hi}$ $CD8^{+}$ T cells from PBMCs of mock- or sequentially-infected mice between 1 and 9 weeks of age. (**E**) Frequency of $GrzB^{+}$ $CD44^{hi}$ $CD8^{+}$ T cells from PBMCs of mock- or sequentially-infected mice between 1 and 9 weeks of age. (**F**) Absolute cell counts of white blood cells (WBC), red blood cells (RBC), platelets (PLT), lymphocytes (Lym), neutrophils (Neu), monocytes (Mon), eosinophils (EOS), and basophils (BAS) in the hematological analysis of mock- (n = 14) and sequentially-infected (n = 15) mice at 7 months of age. Columns show median values, error bars represent the standard error of the mean. In A, significance was determined using unpaired Mann-Whitney test; In B, D E and F, significance was determined using a two-way ANOVA test with the Geisser_Greenhouse correction; In C, significance was determined using Dunn's multiple comparisons correct test: $^{*}p < 0.05$; $^{**}p < 0.01$; $^{***}p < 0.001$; $^{****}p < 0.0001$; ns, not significant.
(TIF)

S3 Fig. Gating strategy for analysis of T cells. (**A**) T cells from mock- (n = 16) or sequentially-infected (n = 21) mice were analyzed at 10 weeks of age. PBMC live single cells were gated for $CD45^{+}$ followed by $CD3^{+}CD4^{+}$ or $CD3^{+}CD8^{+}$ cell populations. $CD44^{lo}/CD62L^{hi}$ (Naive), $CD44^{hi}/CD62L^{hi}$ (antigen-experienced central memory, CM), and $CD44^{hi}/CD62L^{lo}$ (antigen-experienced effector memory, EM) $CD8^{+}$ T cells were evaluated with CD44 and CD62L expression. (**B**) Gating of $KLRG1^{+}$ and GrzB+ cells from $CD44^{hi}$ (antigen-experienced) $CD8^{+}$ T cells from PBMCs of mock- or sequentially-infected mice.
(TIF)

S4 Fig. Sequential viral infections in adult mice beginning at 8 weeks of age stimulates a subset of immune phenotypes. (**A**) Frequency of $CD44^{hi}/CD62L^{lo}$ (antigen-experienced effector memory, EM) $CD8^{+}$ T cell between mock-(n = 11) and sequentially-infected (n = 12) adult mice at 10 weeks post first infection. (**B**) Absolute cell counts of white blood cells (WBC), red blood cells (RBC), platelets (PLT), lymphocytes (Lym), neutrophils (Neu), monocytes (Mon), eosinophils (EOS), and basophils (BAS) in the hematological analysis of mock- (n = 11) and sequentially-infected (n = 12) adult mice at 10 weeks post first infection. Columns show median values, error bars represent the standard error of the mean. Significance was determined using unpaired Mann-Whitney test: $^{*}p < 0.05$; $^{**}p < 0.01$; $^{***}p < 0.001$; $^{****}p < 0.0001$; ns, not significant.
(TIF)

S5 Fig. Gating strategy for tissue immune cell profiling. Ten-week-old mock- and sequentially-infected mice were used to analyze immune cell profiles in different tissues. (A) Splenocytes were gated for lymphocytes (FSC-A/SSC-A), singlets (SSC-W/SSC-H), and T cells (CD3/CD45) followed by CD44+ and tetramer+ cell populations to identify viral-specific T cells. (**B**) Lung cells were gated for lymphocytes (FSC-A/SSC-A), singlets (SSC-W/SSC-H), live cells (Aqua-), CD45+ followed by CD3+ or NK1.1+ cell populations to identify ILC, innate lymphoid cells; T_h, CD4 T helper cells; T_{reg}, regulatory CD4 T cells; γδ T, gamma delta T cells. Single positive staining for T-bet, Gata3, and Rorγt were used to define Th1, Th2, and Th17 lineages, respectively. (**B**) Gating of CD3+ T cells, CD11b+ granulocytes, B1, mature or immature B cells, germinal center (GC) B cells and plasma cells from splenocytes of mock- or sequentially-infected mice. (**C**) Gating of $Lin^{-}Sca1^{+}c\text{-}Kit^{+}$ (LSK), mature or immature B cells, Pre B cells, Pro B cells, and Pre- Pro B cells from bone marrow of mock- or sequentially-infected mice.
(TIF)

S6 Fig. Sequential viral exposure shapes immune cell profiles in tissues. (**A**) Frequency of ILC, innate lymphoid cells; T_h, CD4 T helper cells; T_{reg}, regulatory CD4 T cells; γδ T, gamma delta T cell in the lung and ileum of mock- and sequentially-infected mice at 10 weeks of age. (**B**) Immune cell types isolated and enumerated by flow cytometry from the mesenteric lymph node (MLN) of mock- and sequentially-infected mice, including granulocytes, T cells, B1 cells, B2 cells, mature B cells, immature B cells, GC and plasma cells. (**C**) Frequency of T cells, B1 cells, B2 cells, mature B cells, immature B cells, GC and plasma cells from the spleen as well as the mature B cells, immature B cells, Pre B cells, Pro B cells, Pre-pro B cells, and LSK cells from bone marrow (BM) of mock- and sequentially-infected mice at 10 weeks of age. Columns show median values, error bars represent the standard error of the mean. Significance was determined using unpaired Mann-Whitney test: $^{*}p < 0.05$; $^{**}p < 0.01$; $^{***}p < 0.001$; $^{****}p < 0.0001$; ns, not significant.
(TIF)

S7 Fig. Comparison of intestinal and complete nasal turbinate microbiota between mock- and sequentially-infected mice. (**A, B**) Intestine (mock-: n = 17, sequentially-infected: n = 26) and complete nasal turbinate (mock-: n = 6, sequentially-infected: n = 11) microbiota composition in mock- and sequentially-infected mice at (**A**) phylum and (**B**) species levels. (**C, D**) Relative abundance of potential discriminant taxa from linear discriminant analysis within the (**C**) intestinal and (**D**) complete nasal turbinate at the genus level.
(TIF)

S8 Fig. Gating strategy for post-immunization T cell responses. Ten-week-old mock- and sequentially-infected mice were immunized with ChAd-SARS-CoV-2-S. T cell responses were analyzed in splenocytes at 5 weeks post-vaccination. Cells were gated for lymphocytes (FSC-A/SSC-A), singlets (SSC-W/SSC-H), live cells (Aqua-), CD45+, CD19- followed by CD4+ or CD8+ cell populations expressing IFNγ or granzyme B.
(TIF)

S1 Data. Data underlying Figs 1–6 and S1–S8.
(XLSX)

Acknowledgments

We acknowledge all members of the Baldridge laboratory for helpful discussions. We thank the NIH Tetramer Core Facility (contract number 75N93020D00005) for providing MRV, MNV, and IAV tetramers.

Author Contributions

Conceptualization: Yuhao Li, Jerome M. Molleston, Megan T. Baldridge.

Data curation: Yuhao Li, Megan T. Baldridge.

Formal analysis: Yuhao Li, Crystal Lovato, Megan T. Baldridge.

Funding acquisition: Megan T. Baldridge.

Investigation: Yuhao Li, Jerome M. Molleston, Crystal Lovato, Jasmine Wright, Isabel Erickson, Duyen Bui, Andrew H. Kim, Harshad Ingle, Somya Aggarwal, Lila S. Nolan, Lynne Foster.

Methodology: Yuhao Li, Jerome M. Molleston, Ahmed O. Hassan, Michael S. Diamond, Megan T. Baldridge.

Project administration: Yuhao Li, Megan T. Baldridge.

Resources: Ahmed O. Hassan, Michael S. Diamond, Megan T. Baldridge.

Supervision: Michael S. Diamond, Megan T. Baldridge.

Validation: Yuhao Li, Megan T. Baldridge.

Visualization: Yuhao Li, Megan T. Baldridge.

Writing – original draft: Yuhao Li, Jerome M. Molleston, Megan T. Baldridge.

Writing – review & editing: Yuhao Li, Jerome M. Molleston, Crystal Lovato, Jasmine Wright, Isabel Erickson, Duyen Bui, Andrew H. Kim, Harshad Ingle, Somya Aggarwal, Lila S. Nolan, Ahmed O. Hassan, Lynne Foster, Michael S. Diamond.

References

1. Herati RS, Wherry EJ. What Is the Predictive Value of Animal Models for Vaccine Efficacy in Humans? Consideration of Strategies to Improve the Value of Animal Models. Cold Spring Harb Perspect Biol. 2018; 10(4). Epub 20180402. https://doi.org/10.1101/cshperspect.a031583 PMID: 28348037; PubMed Central PMCID: PMC5880169.
2. Hamilton SE, Badovinac VP, Beura LK, Pierson M, Jameson SC, Masopust D, et al. New Insights into the Immune System Using Dirty Mice. J Immunol. 2020; 205(1):3–11. https://doi.org/10.4049/jimmunol.2000171 PMID: 32571979; PubMed Central PMCID: PMC7316151.
3. Seok J, Warren HS, Cuenca AG, Mindrinos MN, Baker HV, Xu W, et al. Genomic responses in mouse models poorly mimic human inflammatory diseases. Proc Natl Acad Sci U S A. 2013; 110(9):3507–12. Epub 20130211. https://doi.org/10.1073/pnas.1222878110 PMID: 23401516; PubMed Central PMCID: PMC3587220.
4. Mestas J, Hughes CC. Of mice and not men: differences between mouse and human immunology. J Immunol. 2004; 172(5):2731–8. https://doi.org/10.4049/jimmunol.172.5.2731 PMID: 14978070.
5. Huggins MA, Sjaastad FV, Pierson M, Kucaba TA, Swanson W, Staley C, et al. Microbial Exposure Enhances Immunity to Pathogens Recognized by TLR2 but Increases Susceptibility to Cytokine Storm through TLR4 Sensitization. Cell Rep. 2019; 28(7):1729–43 e5. https://doi.org/10.1016/j.celrep.2019.07.028 PMID: 31412243; PubMed Central PMCID: PMC6703181.
6. Beura LK, Hamilton SE, Bi K, Schenkel JM, Odumade OA, Casey KA, et al. Normalizing the environment recapitulates adult human immune traits in laboratory mice. Nature. 2016; 532(7600):512–6. Epub 2016/04/21. https://doi.org/10.1038/nature17655 PMID: 27096360; PubMed Central PMCID: PMC4871315.
7. Masopust D, Sivula CP, Jameson SC. Of Mice, Dirty Mice, and Men: Using Mice To Understand Human Immunology. J Immunol. 2017; 199(2):383–8. https://doi.org/10.4049/jimmunol.1700453 PMID: 28696328; PubMed Central PMCID: PMC5512602.
8. Rosshart SP, Herz J, Vassallo BG, Hunter A, Wall MK, Badger JH, et al. Laboratory mice born to wild mice have natural microbiota and model human immune responses. Science. 2019; 365(6452). Epub 20190801. https://doi.org/10.1126/science.aaw4361 PMID: 31371577; PubMed Central PMCID: PMC7377314.
9. Yeung F, Chen YH, Lin JD, Leung JM, McCauley C, Devlin JC, et al. Altered Immunity of Laboratory Mice in the Natural Environment Is Associated with Fungal Colonization. Cell Host Microbe. 2020; 27(5):809–22 e6. Epub 20200324. https://doi.org/10.1016/j.chom.2020.02.015 PMID: 32209432; PubMed Central PMCID: PMC7276265.
10. Reese TA, Bi K, Kambal A, Filali-Mouhim A, Beura LK, Burger MC, et al. Sequential Infection with Common Pathogens Promotes Human-like Immune Gene Expression and Altered Vaccine Response. Cell Host Microbe. 2016; 19(5):713–9. Epub 20160420. https://doi.org/10.1016/j.chom.2016.04.003 PMID: 27107939; PubMed Central PMCID: PMC4896745.
11. Leung JM, Budischak SA, Chung The H, Hansen C, Bowcutt R, Neill R, et al. Rapid environmental effects on gut nematode susceptibility in rewilded mice. PLoS Biol. 2018; 16(3):e2004108. Epub 20180308. https://doi.org/10.1371/journal.pbio.2004108 PMID: 29518091; PubMed Central PMCID: PMC5843147.
12. Fiege JK, Block KE, Pierson MJ, Nanda H, Shepherd FK, Mickelson CK, et al. Mice with diverse microbial exposure histories as a model for preclinical vaccine testing. Cell Host Microbe. 2021. Epub 2021/11/04. https://doi.org/10.1016/j.chom.2021.10.001 PMID: 34731647.

13. Li Y, Baldridge MT. Modelling human immune responses using microbial exposures in rodents. Nat Microbiol. 2023; 8(3):363–6. https://doi.org/10.1038/s41564-023-01334-w PMID: 36797488; PubMed Central PMCID: PMC9992131.
14. Fiege JK, Langlois RA. Embracing the heterogeneity of natural viruses in mouse studies. J Gen Virol. 2022; 103(6). https://doi.org/10.1099/jgv.0.001758 PMID: 35737518; PubMed Central PMCID: PMC10027023.
15. Fay EJ, Balla KM, Roach SN, Shepherd FK, Putri DS, Wiggen TD, et al. Natural rodent model of viral transmission reveals biological features of virus population dynamics. J Exp Med. 2022; 219(2). Epub 20211227. https://doi.org/10.1084/jem.20211220 PMID: 34958350; PubMed Central PMCID: PMC8713297.
16. Midha A, Jarquin-Diaz VH, Ebner F, Lober U, Hayani R, Kundik A, et al. Guts within guts: the microbiome of the intestinal helminth parasite Ascaris suum is derived but distinct from its host. Microbiome. 2022; 10(1):229. Epub 20221216. https://doi.org/10.1186/s40168-022-01399-5 PMID: 36527132; PubMed Central PMCID: PMC9756626.
17. Llinas-Caballero K, Caraballo L. Helminths and Bacterial Microbiota: The Interactions of Two of Humans' "Old Friends". Int J Mol Sci. 2022; 23(21). Epub 20221101. https://doi.org/10.3390/ijms232113358 PMID: 36362143; PubMed Central PMCID: PMC9658883.
18. Rivera-Gutierrez X, Moran P, Taboada B, Serrano-Vazquez A, Isa P, Rojas-Velazquez L, et al. The fecal and oropharyngeal eukaryotic viromes of healthy infants during the first year of life are personal. Sci Rep. 2023; 13(1):938. Epub 20230117. https://doi.org/10.1038/s41598-022-26707-9 PMID: 36650178; PubMed Central PMCID: PMC9845211.
19. Zheng QY, Huynh KT, van Zuylen WJ, Craig ME, Rawlinson WD. Cytomegalovirus infection in day care centres: A systematic review and meta-analysis of prevalence of infection in children. Rev Med Virol. 2019; 29(1):e2011. Epub 20181010. https://doi.org/10.1002/rmv.2011 PMID: 30306730.
20. de-The G, Day NE, Geser A, Lavoue MF, Ho JH, Simons MJ, et al. Sero-epidemiology of the Epstein-Barr virus: preliminary analysis of an international study—a review. IARC Sci Publ (1971). 1975;(11 Pt 2):3–16. PMID: 191375
21. Farkas T, Fey B, Keller G, Martella V, Egyed L. Molecular detection of murine noroviruses in laboratory and wild mice. Vet Microbiol. 2012; 160(3–4):463–7. Epub 20120613. https://doi.org/10.1016/j.vetmic.2012.06.002 PMID: 22748629; PubMed Central PMCID: PMC3469783.
22. Shah MP, Hall AJ. Norovirus Illnesses in Children and Adolescents. Infect Dis Clin North Am. 2018; 32(1):103–18. https://doi.org/10.1016/j.idc.2017.11.004 PMID: 29406972; PubMed Central PMCID: PMC6814392.
23. Hebbelstrup Jensen B, Jokelainen P, Nielsen ACY, Franck KT, Rejkjaer Holm D, Schonning K, et al. Children Attending Day Care Centers are a Year-round Reservoir of Gastrointestinal Viruses. Sci Rep. 2019; 9(1):3286. Epub 20190301. https://doi.org/10.1038/s41598-019-40077-9 PMID: 30824842; PubMed Central PMCID: PMC6397223.
24. Ruf BR, Knuf M. The burden of seasonal and pandemic influenza in infants and children. Eur J Pediatr. 2014; 173(3):265–76. Epub 20130510. https://doi.org/10.1007/s00431-013-2023-6 PMID: 23661234; PubMed Central PMCID: PMC3930829.
25. El Guerche-Seblain C, Moureau A, Schiffler C, Dupuy M, Pepin S, Samson SI, et al. Epidemiology and burden of influenza in healthy children aged 6 to 35 months: analysis of data from the placebo arm of a phase III efficacy trial. BMC Infect Dis. 2019; 19(1):308. Epub 20190404. https://doi.org/10.1186/s12879-019-3920-8 PMID: 30947693; PubMed Central PMCID: PMC6449994.
26. Morita H, Yasuda M, Yamamoto M, Uchida R, Tanaka M, Ishida T, et al. Prevalence of murine astrovirus in laboratory animal facilities in Japan. J Vet Med Sci. 2020; 82(7):881–5. Epub 20200518. https://doi.org/10.1292/jvms.20-0180 PMID: 32418936; PubMed Central PMCID: PMC7399306.
27. Jeong HS, Jeong A, Cheon DS. Epidemiology of astrovirus infection in children. Korean J Pediatr. 2012; 55(3):77–82. Epub 20120316. https://doi.org/10.3345/kjp.2012.55.3.77 PMID: 22474461; PubMed Central PMCID: PMC3315622.
28. Shrestha SK, Shrestha J, Andreassen AK, Strand TA, Dudman S, Dembinski JL. Genetic Diversity of Astrovirus in Children From a Birth Cohort in Nepal. Front Microbiol. 2020; 11:588707. Epub 20210205. https://doi.org/10.3389/fmicb.2020.588707 PMID: 33613461; PubMed Central PMCID: PMC7893100.
29. Brouwer L, Moreni G, Wolthers KC, Pajkrt D. World-Wide Prevalence and Genotype Distribution of Enteroviruses. Viruses. 2021; 13(3). Epub 20210308. https://doi.org/10.3390/v13030434 PMID: 33800518; PubMed Central PMCID: PMC7999254.
30. Prill MM, Dahl RM, Midgley CM, Chern SW, Lu X, Feikin DR, et al. Severe Respiratory Illness Associated With Rhinovirus During the Enterovirus D68 Outbreak in the United States, August 2014-November 2014. Clin Infect Dis. 2018; 66(10):1528–34. https://doi.org/10.1093/cid/cix1034 PMID: 29186347.

31. Baldridge MT, Nice TJ, McCune BT, Yokoyama CC, Kambal A, Wheadon M, et al. Commensal microbes and interferon-lambda determine persistence of enteric murine norovirus infection. Science. 2015; 347(6219):266–9. Epub 20141127. https://doi.org/10.1126/science.1258025 PMID: 25431490; PubMed Central PMCID: PMC4409937.

32. Ingle H, Hassan E, Gawron J, Mihi B, Li Y, Kennedy EA, et al. Murine astrovirus tropism for goblet cells and enterocytes facilitates an IFN-lambda response in vivo and in enteroid cultures. Mucosal Immunol. 2021; 14(3):751–61. Epub 20210305. https://doi.org/10.1038/s41385-021-00387-6 PMID: 33674763; PubMed Central PMCID: PMC8085034.

33. Shi Z, Zou J, Zhang Z, Zhao X, Noriega J, Zhang B, et al. Segmented Filamentous Bacteria Prevent and Cure Rotavirus Infection. Cell. 2019; 179(3):644–58 e13. Epub 20191010. https://doi.org/10.1016/j.cell.2019.09.028 PMID: 31607511; PubMed Central PMCID: PMC7525827.

34. Dhalech AH, Corn CM, Mangale V, Syed F, Condotta SA, Richer MJ, et al. Testosterone Promotes the Intestinal Replication and Dissemination of Coxsackievirus B3 in an Oral Inoculation Mouse Model. J Virol. 2022; 96(17):e0123222. Epub 20220829. https://doi.org/10.1128/jvi.01232-22 PMID: 36037480; PubMed Central PMCID: PMC9472648.

35. Langdon JM, Yates SC, Femnou LK, McCranor BJ, Cheadle C, Xue QL, et al. Hepcidin-dependent and hepcidin-independent regulation of erythropoiesis in a mouse model of anemia of chronic inflammation. Am J Hematol. 2014; 89(5):470–9. Epub 20140224. https://doi.org/10.1002/ajh.23670 PMID: 24415655; PubMed Central PMCID: PMC4200395.

36. Beura LK, Wijeyesinghe S, Thompson EA, Macchietto MG, Rosato PC, Pierson MJ, et al. T Cells in Nonlymphoid Tissues Give Rise to Lymph-Node-Resident Memory T Cells. Immunity. 2018; 48(2):327–38 e5. https://doi.org/10.1016/j.immuni.2018.01.015 PMID: 29466758; PubMed Central PMCID: PMC5828517.

37. Muleta KG, Ulmert I, Hamza KH, van Dijl S, Nakawesi J, Lahl K. Rotavirus-Induced Expansion of Antigen-Specific CD8 T Cells Does Not Require Signaling via TLR3, MyD88 or the Type I Interferon Receptor. Front Immunol. 2022; 13:814491. Epub 20220407. https://doi.org/10.3389/fimmu.2022.814491 PMID: 35464475; PubMed Central PMCID: PMC9022177.

38. Tomov VT, Osborne LC, Dolfi DV, Sonnenberg GF, Monticelli LA, Mansfield K, et al. Persistent enteric murine norovirus infection is associated with functionally suboptimal virus-specific CD8 T cell responses. J Virol. 2013; 87(12):7015–31. Epub 20130417. https://doi.org/10.1128/JVI.03389-12 PMID: 23596300; PubMed Central PMCID: PMC3676130.

39. Si Y, Wen Y, Kelly SH, Chong AS, Collier JH. Intranasal delivery of adjuvant-free peptide nanofibers elicits resident CD8(+) T cell responses. J Control Release. 2018; 282:120–30. Epub 20180417. https://doi.org/10.1016/j.jconrel.2018.04.031 PMID: 29673645; PubMed Central PMCID: PMC6309200.

40. Tomov VT, Palko O, Lau CW, Pattekar A, Sun Y, Tacheva R, et al. Differentiation and Protective Capacity of Virus-Specific CD8(+) T Cells Suggest Murine Norovirus Persistence in an Immune-Privileged Enteric Niche. Immunity. 2017; 47(4):723–38 e5. Epub 20171011. https://doi.org/10.1016/j.immuni.2017.09.017 PMID: 29031786; PubMed Central PMCID: PMC6077984.

41. Hassan AO, Kafai NM, Dmitriev IP, Fox JM, Smith BK, Harvey IB, et al. A Single-Dose Intranasal ChAd Vaccine Protects Upper and Lower Respiratory Tracts against SARS-CoV-2. Cell. 2020; 183(1):169–84 e13. Epub 20200819. https://doi.org/10.1016/j.cell.2020.08.026 PMID: 32931734; PubMed Central PMCID: PMC7437481.

42. Case JB, Rothlauf PW, Chen RE, Liu Z, Zhao H, Kim AS, et al. Neutralizing Antibody and Soluble ACE2 Inhibition of a Replication-Competent VSV-SARS-CoV-2 and a Clinical Isolate of SARS-CoV-2. Cell Host Microbe. 2020; 28(3):475–85 e5. Epub 20200703. https://doi.org/10.1016/j.chom.2020.06.021 PMID: 32735849; PubMed Central PMCID: PMC7332453.

43. Grifoni A, Weiskopf D, Ramirez SI, Mateus J, Dan JM, Moderbacher CR, et al. Targets of T Cell Responses to SARS-CoV-2 Coronavirus in Humans with COVID-19 Disease and Unexposed Individuals. Cell. 2020; 181(7):1489–501 e15. Epub 20200520. https://doi.org/10.1016/j.cell.2020.05.015 PMID: 32473127; PubMed Central PMCID: PMC7237901.

44. Nakaya HI, Hagan T, Duraisingham SS, Lee EK, Kwissa M, Rouphael N, et al. Systems Analysis of Immunity to Influenza Vaccination across Multiple Years and in Diverse Populations Reveals Shared Molecular Signatures. Immunity. 2015; 43(6):1186–98. https://doi.org/10.1016/j.immuni.2015.11.012 PMID: 26682988; PubMed Central PMCID: PMC4859820.

45. Payton T, Girgenti D, Frenck RW, Patterson S, Love J, Razmpour A, et al. Immunogenicity, safety and tolerability of 3 lots of 13-valent pneumococcal conjugate vaccine given with routine pediatric vaccinations in the United States. Pediatr Infect Dis J. 2013; 32(8):871–80. https://doi.org/10.1097/INF.0b013e3182906499 PMID: 23584582.

46. Barouch DH, Tomaka FL, Wegmann F, Stieh DJ, Alter G, Robb ML, et al. Evaluation of a mosaic HIV-1 vaccine in a multicentre, randomised, double-blind, placebo-controlled, phase 1/2a clinical trial (APPROACH) and in rhesus monkeys (NHP 13–19). Lancet. 2018; 392(10143):232–43. Epub

20180706. https://doi.org/10.1016/S0140-6736(18)31364-3 PMID: 30047376; PubMed Central PMCID: PMC6192527.

47. Lynn DJ, Benson SC, Lynn MA, Pulendran B. Modulation of immune responses to vaccination by the microbiota: implications and potential mechanisms. Nat Rev Immunol. 2022; 22(1):33–46. Epub 20210517. https://doi.org/10.1038/s41577-021-00554-7 PMID: 34002068; PubMed Central PMCID: PMC8127454.

48. Dbaibo G, Amanullah A, Claeys C, Izu A, Jain VK, Kosalaraksa P, et al. Quadrivalent Influenza Vaccine Prevents Illness and Reduces Healthcare Utilization Across Diverse Geographic Regions During Five Influenza Seasons: A Randomized Clinical Trial. Pediatr Infect Dis J. 2020; 39(1):e1–e10. https://doi.org/10.1097/INF.0000000000002504 PMID: 31725115; PubMed Central PMCID: PMC7004464.

49. Muyanja E, Ssemaganda A, Ngauv P, Cubas R, Perrin H, Srinivasan D, et al. Immune activation alters cellular and humoral responses to yellow fever 17D vaccine. J Clin Invest. 2014; 124(7):3147–58. Epub 20140609. https://doi.org/10.1172/JCI75429 PMID: 24911151; PubMed Central PMCID: PMC4071376.

50. Pasin C, Balelli I, Van Effelterre T, Bockstal V, Solforosi L, Prague M, et al. Dynamics of the Humoral Immune Response to a Prime-Boost Ebola Vaccine: Quantification and Sources of Variation. J Virol. 2019; 93(18). Epub 20190828. https://doi.org/10.1128/JVI.00579-19 PMID: 31243126; PubMed Central PMCID: PMC6714808.

51. de Jong SE, Olin A, Pulendran B. The Impact of the Microbiome on Immunity to Vaccination in Humans. Cell Host Microbe. 2020; 28(2):169–79. https://doi.org/10.1016/j.chom.2020.06.014 PMID: 32791110; PubMed Central PMCID: PMC7422826.

52. Oh JZ, Ravindran R, Chassaing B, Carvalho FA, Maddur MS, Bower M, et al. TLR5-mediated sensing of gut microbiota is necessary for antibody responses to seasonal influenza vaccination. Immunity. 2014; 41(3):478–92. Epub 20140911. https://doi.org/10.1016/j.immuni.2014.08.009 PMID: 25220212; PubMed Central PMCID: PMC4169736.

53. Hagan T, Cortese M, Rouphael N, Boudreau C, Linde C, Maddur MS, et al. Antibiotics-Driven Gut Microbiome Perturbation Alters Immunity to Vaccines in Humans. Cell. 2019; 178(6):1313–28 e13. https://doi.org/10.1016/j.cell.2019.08.010 PMID: 31491384; PubMed Central PMCID: PMC6750738.

54. Kim AH, Armah G, Dennis F, Wang L, Rodgers R, Droit L, et al. Enteric virome negatively affects seroconversion following oral rotavirus vaccination in a longitudinally sampled cohort of Ghanaian infants. Cell Host Microbe. 2022; 30(1):110–23 e5. Epub 20211220. https://doi.org/10.1016/j.chom.2021.12.002 PMID: 34932985; PubMed Central PMCID: PMC8763403.

55. Harris VC, Haak BW, Handley SA, Jiang B, Velasquez DE, Hykes BL Jr., et al. Effect of Antibiotic-Mediated Microbiome Modulation on Rotavirus Vaccine Immunogenicity: A Human, Randomized-Control Proof-of-Concept Trial. Cell Host Microbe. 2018; 24(2):197–207 e4. https://doi.org/10.1016/j.chom.2018.07.005 PMID: 30092197.

56. Ng SC, Peng Y, Zhang L, Mok CK, Zhao S, Li A, et al. Gut microbiota composition is associated with SARS-CoV-2 vaccine immunogenicity and adverse events. Gut. 2022; 71(6):1106–16. Epub 20220209. https://doi.org/10.1136/gutjnl-2021-326563 PMID: 35140064; PubMed Central PMCID: PMC8844967.

57. Akatsu H, Iwabuchi N, Xiao JZ, Matsuyama Z, Kurihara R, Okuda K, et al. Clinical effects of probiotic Bifidobacterium longum BB536 on immune function and intestinal microbiota in elderly patients receiving enteral tube feeding. JPEN J Parenter Enteral Nutr. 2013; 37(5):631–40. Epub 20121127. https://doi.org/10.1177/0148607112467819 PMID: 23192454.

58. Wu BB, Yang Y, Xu X, Wang WP. Effects of Bifidobacterium supplementation on intestinal microbiota composition and the immune response in healthy infants. World J Pediatr. 2016; 12(2):177–82. Epub 20150406. https://doi.org/10.1007/s12519-015-0025-3 PMID: 25846071.

59. Bosch M, Mendez M, Perez M, Farran A, Fuentes MC, Cune J. Lactobacillus plantarum CECT7315 and CECT7316 stimulate immunoglobulin production after influenza vaccination in elderly. Nutr Hosp. 2012; 27(2):504–9. https://doi.org/10.1590/S0212-16112012000200023 PMID: 22732975.

60. Barton ES, White DW, Cathelyn JS, Brett-McClellan KA, Engle M, Diamond MS, et al. Herpesvirus latency confers symbiotic protection from bacterial infection. Nature. 2007; 447(7142):326–9. https://doi.org/10.1038/nature05762 PMID: 17507983.

61. Stelekati E, Wherry EJ. Chronic bystander infections and immunity to unrelated antigens. Cell Host Microbe. 2012; 12(4):458–69. https://doi.org/10.1016/j.chom.2012.10.001 PMID: 23084915; PubMed Central PMCID: PMC3617576.

62. Hassan AO, Shrihari S, Gorman MJ, Ying B, Yuan D, Raju S, et al. An intranasal vaccine durably protects against SARS-CoV-2 variants in mice. Cell Rep. 2021; 36(4):109452. Epub 20210710. https://doi.org/10.1016/j.celrep.2021.109452 PMID: 34289385; PubMed Central PMCID: PMC8270739.

63. Hoffmann M, Kleine-Weber H, Schroeder S, Kruger N, Herrler T, Erichsen S, et al. SARS-CoV-2 Cell Entry Depends on ACE2 and TMPRSS2 and Is Blocked by a Clinically Proven Protease Inhibitor. Cell. 2020; 181(2):271–80 e8. Epub 20200305. https://doi.org/10.1016/j.cell.2020.02.052 PMID: 32142651; PubMed Central PMCID: PMC7102627.

64. Caporaso JG, Lauber CL, Walters WA, Berg-Lyons D, Lozupone CA, Turnbaugh PJ, et al. Global patterns of 16S rRNA diversity at a depth of millions of sequences per sample. Proc Natl Acad Sci U S A. 2011; 108 Suppl 1:4516–22. Epub 2010/06/11. https://doi.org/10.1073/pnas.1000080107 PMID: 20534432; PubMed Central PMCID: PMC3063599.

65. Callahan BJ, McMurdie PJ, Rosen MJ, Han AW, Johnson AJ, Holmes SP. DADA2: High-resolution sample inference from Illumina amplicon data. Nat Methods. 2016; 13(7):581–3. Epub 2016/05/24. https://doi.org/10.1038/nmeth.3869 PMID: 27214047; PubMed Central PMCID: PMC4927377.

66. Cole JR, Wang Q, Fish JA, Chai B, McGarrell DM, Sun Y, et al. Ribosomal Database Project: data and tools for high throughput rRNA analysis. Nucleic Acids Res. 2014; 42(Database issue):D633–42. Epub 2013/11/30. https://doi.org/10.1093/nar/gkt1244 PMID: 24288368; PubMed Central PMCID: PMC3965039.

67. McMurdie PJ, Holmes S. phyloseq: an R package for reproducible interactive analysis and graphics of microbiome census data. PLoS One. 2013; 8(4):e61217. Epub 2013/05/01. https://doi.org/10.1371/journal.pone.0061217 PMID: 23630581; PubMed Central PMCID: PMC3632530.

68. Xu S, Zhan L, Tang W, Wang Q, Dai Z, Zhou L, et al. MicrobiotaProcess: A comprehensive R package for deep mining microbiome. Innovation (Camb). 2023; 4(2):100388. Epub 20230202. https://doi.org/10.1016/j.xinn.2023.100388 PMID: 36895758; PubMed Central PMCID: PMC9988672.

69. Segata N, Izard J, Waldron L, Gevers D, Miropolsky L, Garrett WS, et al. Metagenomic biomarker discovery and explanation. Genome Biol. 2011; 12(6):R60. Epub 2011/06/28. https://doi.org/10.1186/gb-2011-12-6-r60 PMID: 21702898; PubMed Central PMCID: PMC3218848.

70. Baert L, Wobus CE, Van Coillie E, Thackray LB, Debevere J, Uyttendaele M. Detection of murine norovirus 1 by using plaque assay, transfection assay, and real-time reverse transcription-PCR before and after heat exposure. Appl Environ Microbiol. 2008; 74(2):543–6. Epub 2007/11/21. https://doi.org/10.1128/AEM.01039-07 PMID: 18024676; PubMed Central PMCID: PMC2223245.

71. Ingle H, Lee S, Ai T, Orvedahl A, Rodgers R, Zhao G, et al. Viral complementation of immunodeficiency confers protection against enteric pathogens via interferon-lambda. Nat Microbiol. 2019; 4(7):1120–8. Epub 2019/04/03. https://doi.org/10.1038/s41564-019-0416-7 PMID: 30936486; PubMed Central PMCID: PMC6588490.

72. Baldridge MT, Lee S, Brown JJ, McAllister N, Urbanek K, Dermody TS, et al. Expression of Ifnlr1 on intestinal epithelial cells is critical to the antiviral effects of IFN-lambda against norovirus and reovirus. J Virol. 2017. https://doi.org/10.1128/JVI.02079-16 PMID: 28077655.

73. Nakazawa M. fmsb: Functions for medical statistics book with some demographic data. R package version 06. 2018; 3(3).